

Models of crustal flow in the India–Asia collision zone

Alex Copley¹ and Dan McKenzie²

¹COMET, Department of Earth Sciences, University of Cambridge, Cambridge, UK. E-mail: copley@esc.cam.ac.uk

²Department of Earth Sciences, University of Cambridge, Cambridge, UK

Accepted 2007 January 2. Received 2006 December 21; in original form 2006 June 6

SUMMARY

Surface velocities in parts of the India–Asia collision zone are compared to velocities calculated from equations describing fluid flow driven by topographically produced pressure gradients. A good agreement is found if the viscosity of the crust is $\sim 10^{20}$ Pa s in southern Tibet and $\sim 10^{22}$ Pa s in the area between the Eastern Syntaxis and the Szechwan Basin. The lower boundary condition of the flow changes between these two areas, with a stress-free lower boundary in the area between the Szechwan basin and the Eastern Syntaxis, and a horizontally rigid but vertically deformable boundary where strong Indian lithospheric material underlies southern Tibet. Deformation maps for olivine, diopside and anorthite show our findings to be consistent with laboratory measurements of the rheology of minerals. Gravitationally driven flow is also suggested to be taking place in the Indo–Burman Ranges, with a viscosity of $\sim 10^{19}$ – 10^{20} Pa s. Flow in both southern Tibet and the Indo–Burman Ranges provides an explanation for the formation of the geometry of the Eastern Himalayan Syntaxis. The majority of the normal faulting earthquakes in the Tibetan Plateau occur in the area of southern Tibet which we model as gravitationally spreading over the Indian shield.

Key words: continental deformation, gravity, rheology, topography.

1 INTRODUCTION

At temperatures greater than around two thirds of the melting temperature, minerals can deform by thermally activated creep at geologically significant strain-rates. In areas where the lower crust is hot either because the crust is thick or the heat flux is high, it can deform by creep at high enough rates to behave as a fluid on geological timescales. Lower crustal flow has been suggested as an explanation for the absence of Moho topography in regions where the upper crust is highly strained, such as the Basin and Range province of the western United States (e.g. Block & Royden 1990; Kruse *et al.* 1991; McKenzie *et al.* 2000). Shapiro *et al.* (2004) used the dispersion of surface waves to suggest that significant anisotropy exists in the Tibetan crust, which they interpret as the result of lower crustal flow. Crustal flow has also been suggested as a cause of the low relief in the interior of the Tibetan Plateau (e.g. Fielding *et al.* 1994). Motivated by the indications that flow is occurring in the Tibetan crust, in this paper we calculate surface velocities for southern Tibet and the area between the Eastern Syntaxis and the Szechwan Basin (Fig. 1) using equations for fluid flow. The results of these calculations are in agreement with published GPS measurements. Under the assumption that deformation is occurring by diffusion creep in the thick sequence of sediments, we also model the deformation of the Indo–Burman Ranges as that of a viscous fluid. Deformation maps have been created to test if the viscosities which we calculate for the crust in Tibet are consistent with the rheology of minerals. These deformation maps have also been used to deduce the domi-

nant mechanism of creep likely to be operating in the ductile part of the crust, and so determine the rheology used in our models.

2 MODEL AND RELATION TO PREVIOUS WORK

The study of continental deformation and crustal flow using the equations for fluid flow has been undertaken using a number of different methods and boundary conditions. Throughout this paper we take ‘stress-free’ to mean that the shear stress on the boundary of a layer is zero, and there is no restriction on the horizontal velocity. By ‘rigid’ we mean that the horizontal velocity is zero. A boundary is described as undeformable if the vertical velocity is zero, and as deformable if the normal stress is continuous. A boundary may be both rigid and deformable if the horizontal velocity is zero, but the vertical velocity is not.

England & McKenzie (1982) modelled the continental lithosphere as a thin sheet of power-law fluid overlying an inviscid half-space. England & Houseman (1986) compared the predictions of this model to topography and strain within the India–Asia collision zone. This model assumes that vertical gradients of horizontal velocity are negligible, and uses stress-free upper and lower boundary conditions.

Royden (1996) studied the basally driven flow of a Newtonian fluid with depth-dependent viscosity and described two end-member situations, where the deformation of the crust is coupled to, or decoupled from, the motion in an upper mantle with a specified horizontal

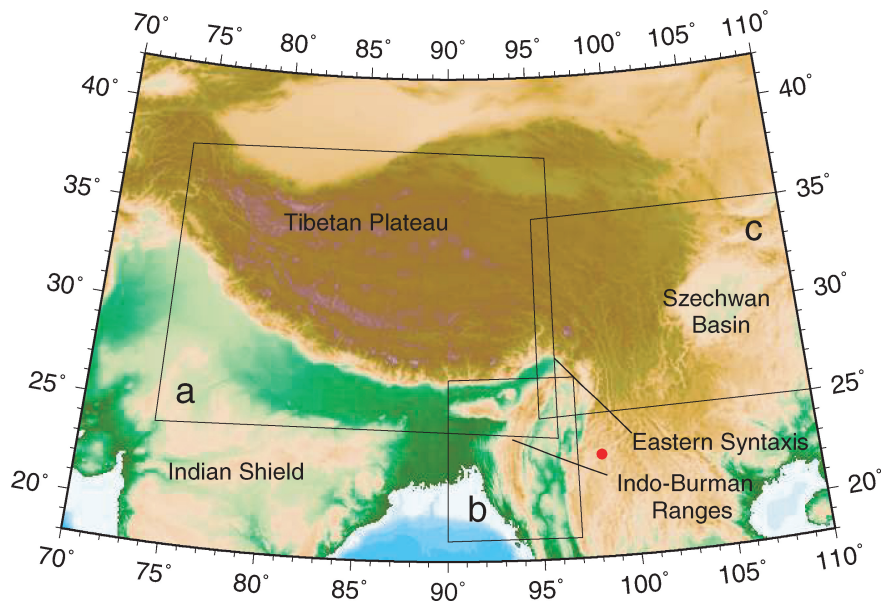


Figure 1. Topography of the Tibetan Plateau and surrounding regions. Box a shows the area pictured in Fig. 2, box b shows the location of Fig. 4 and box c shows the area of coverage of Fig. 7(a). The red circle represents the pole to which the Indo–Burman Ranges approximate an arc of a small-circle (Section 4).

velocity. Shen *et al.* (2001) compared topography and surface motions from this model to observations of the Tibetan Plateau. These authors use a fixed-horizontal-velocity lower boundary and a stress-free upper boundary, both of which are deformable.

Zhao & Morgan (1987) used rigid and deformable upper and lower boundaries to model the injection of Indian crustal material into the lower crust of Tibet. Clark & Royden (2000) used rigid upper and lower boundaries to model flow in a lower crustal channel of uniform width. Bird (1991) studied the lateral extrusion of the lower crust driven by pressure gradients resulting from topographic gradients. His model has a power-law rheology and a depth-dependent viscosity. He used a rigid lower boundary condition, and his assumed rheology effectively created a rigid upper boundary condition to a lower-crustal channel. Beaumont *et al.* (2001) used a temperature-dependent viscosity for crustal flow which had the effect of confining flow to a lower crustal channel. Clark *et al.* (2005) studied flow in a channel with fixed horizontal boundaries overlain by an elastic layer which can deform in response to flow in the channel, and suggested that rheological heterogeneities can account for some of the topography in eastern Tibet.

M^cKenzie *et al.* (2000) studied the response of a viscous layer overlying a viscous half-space to an instantaneous perturbation, and obtained expressions for the timescales involved in the decay of topography on the upper and lower boundaries of the layer for continuous stress and rigid lower boundary conditions. They also extended the analysis of Huppert (1982), who studied the propagation of gravity currents over a rigid horizontal surface, to include isostatically compensated gravity currents with a rigid and deformable lower boundary condition. They showed that the form of the flow was similar if one or both of the horizontal boundaries were rigid, and that it did not matter which boundary was the rigid one. This is because the rigidity of either boundary means that any flow which occurs involves relatively large vertical gradients of horizontal velocity. These flows take a very different form to those in which both upper and lower boundaries are stress-free.

We have chosen to use the simplest models which are likely to include the important features of crustal flow, rather than more complex models involving many (sometimes poorly known) parameters.

We use a constant viscosity fluid, which means the viscosities we calculate will represent some vertical average of the actual viscosity. Gravity and earthquake data (M^cKenzie & Fairhead 1997; Jackson 2002) suggest that the Indian crust is unusually strong. Therefore, as described below, we model the flow of crustal material over India from the north (Tibet) and east (the Indo–Burman Ranges) as flows with stress-free upper surfaces and rigid but deformable bases, using the approach of M^cKenzie *et al.* (2000). We allow the base to deform vertically in order to maintain isostatic equilibrium. Because the Indo–Burman Ranges may not be isostatically compensated (e.g. Verma *et al.* 1976), in this area we also consider a gently dipping stationary lower boundary. Unlike southern Tibet, there is no evidence for a rigid substrate underlying the area between the Szechwan Basin and the Eastern Syntaxis, so the motion of material in this area is modelled as a flow with stress-free upper and lower surfaces. The lowlands bordering the plateau in this area have low elevation and relief, and are likely to be relatively rigid, so we impose zero-velocity conditions on the edges of the flow. The upper and lower boundary conditions in this area are the same as used in the ‘thin viscous sheet’ models, but we impose zero-velocity conditions on the edges of the flow, and hope to gain further insight by studying a relatively small area and comparing our model to a well-determined velocity field, rather than attempting to model the entire orogenic zone. Stress-free upper boundary conditions have been used in all our models because considerable divergence of surface velocities (e.g. in fig. 6 of Holt *et al.* 2000), and plentiful earthquake activity suggest the use of a boundary which is not rigid.

3 SOUTHERN TIBET

In this section, we model the southern Tibetan Plateau as a gravitationally driven flow propagating southwards and overriding the Indian lithosphere, and compare our results to geodetically observed surface velocities (Jade *et al.* 2004; Zhang *et al.* 2004). This approach is motivated by a number of observations from southern Tibet. First, Huang *et al.* (2000) record significant seismic anisotropy in the lithosphere north of $\sim 32^\circ\text{N}$, and largely isotropic lithosphere further south, which is a property also shown by the lithosphere of

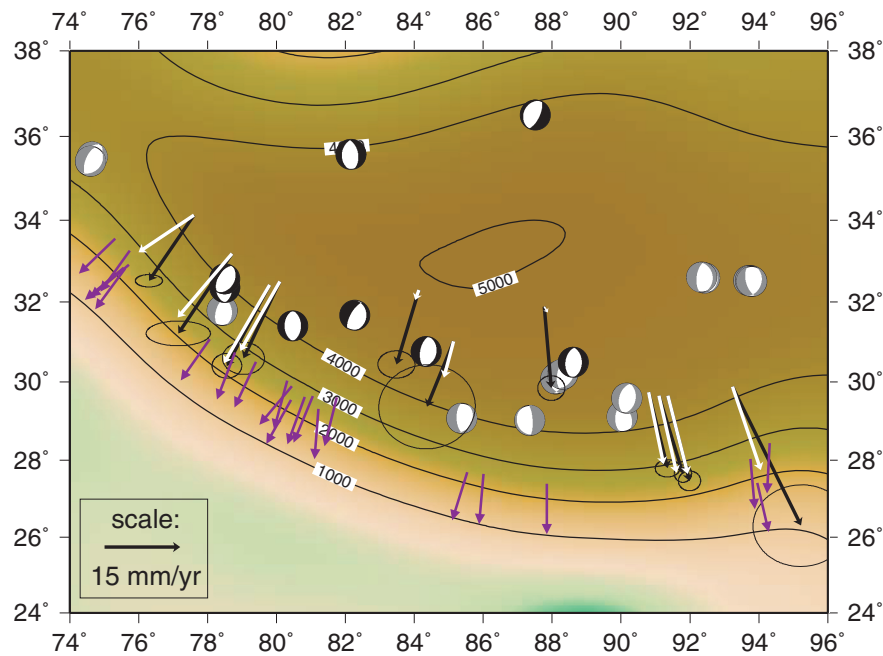


Figure 2. Long-wavelength topography of Tibet (created by low-pass filtering the topography using a radial Gaussian filter with a diameter of 1000 km). Contours show the elevation in metres. Also pictured are model (white) and GPS (Jade *et al.* 2004; Zhang *et al.* 2004) (black) surface velocities relative to India. Error ellipses are 2σ . The model velocities were calculated using a viscosity of 1.7×10^{20} Pa s, a value of f of 7 and using topography filtered with a radial Gaussian filter of diameter 1000 km. The two GPS sites closest to the 5000 m contour are too far from the plateau edges to be affected by the flow which we model, and show effectively zero model velocities. The other sites pictured are the ones used when calculating the misfit between the model and GPS velocities (Fig. 3). For clarity we have omitted those GPS sites near the southern margin of the plateau which we have not modelled because they are affected by elastic deformation from the thrust faults around the edge of the plateau, and also most of those in the central/northern plateau which are not affected by the flow which we model. Also pictured are the focal mechanisms of normal faulting earthquakes within the plateau (those with magnitudes greater than 5.5, and rakes within 30° of -90°) from the CMT catalogue (grey) and from Molnar & Chen (1983), Molnar & Lyon-Caen (1989) (black). CMT focal mechanisms are only shown for those earthquakes with more than 80 per cent double couple, where the percentage double couple of an earthquake is taken to be $\gamma = 100\{1 - [(2|\lambda_2| \times 1.5)/(|\lambda_1| + |\lambda_3|)]\}$, where λ_1 , λ_2 and λ_3 are defined to be the maximum, intermediate and minimum eigenvalues of the moment tensor, and is a measure of how well the moment tensor approximates a double couple. See Jackson *et al.* (2002) for a fuller description. The purple arrows on the edge of the plateau show the slip vectors for earthquakes which occurred on low-angle thrusts (from CMT solutions with more than 80 per cent double couple and Baranowski *et al.* 1984; Molnar *et al.* 1977; Molnar & Lyon-Caen 1989; Chen & Kao 1996).

India. Hoke *et al.* (2000) analysed geothermal helium emissions, and found significant mantle-derived He^3 was present only north of $\sim 30^\circ\text{N}$. They interpret this change to mark the northern limit of Indian lithospheric material beneath the plateau. Jin *et al.* (1996) use gravity anomalies to suggest the northern limit of Indian material lies at $\sim 33^\circ\text{N}$. These studies all suggest that the southern portion of the Tibetan Plateau is underlain by Indian lithospheric material. Secondly, earthquakes which have occurred on low-angle thrusts around the edges of the plateau show slip vectors oriented radially to the arc (Fig. 2), down the local topographic gradient, in the direction of gravitationally driven fluid flow, which is always down the surface gradient of the flow. Thirdly, it is likely that the temperature in the crust overlying the Indian lithosphere is high enough that flow will occur on geological timescales (e.g. Hacker *et al.* 2000; Lee *et al.* 2004; Mechie *et al.* 2004). Shapiro *et al.* (2004) and Fielding *et al.* (1994) also suggest crustal flow is occurring in the Tibetan Plateau.

Gravity and earthquake data (e.g. M^cKenzie & Fairhead 1997; Jackson 2002) suggest that the Indian crust is unusually strong, so is likely to provide a lower boundary which has zero horizontal velocity (in an India-relative reference frame) but can deform vertically to maintain isostatic equilibrium, so we choose a rigid and deformable lower boundary condition.

M^cKenzie *et al.* (2000) derived the equations for an isostatically compensated gravity current of less dense material propagating over a more dense material with zero horizontal velocity on the interface.

M^cKenzie *et al.* (2000) assume that the horizontal extent of the flow is much greater than the thickness. This, in conjunction with the horizontally rigid base to the flow, means that the dominant velocity gradients are the vertical gradients of horizontal velocity. In southern Tibet the surface velocities in an India-relative reference frame are mostly $15\text{--}20\text{ mm yr}^{-1}$. The top of the Indian lithospheric material is thought to be at around $\sim 50\text{ km}$ (e.g. Owens & Zandt 1997), at which depth the velocity in an India-relative frame will be approximately zero. This vertical velocity gradient is much larger than any other velocity gradients in the area, supporting the use of the equations of M^cKenzie *et al.* (2000). If one or both of the horizontal boundaries of a gravity current have zero horizontal velocity and the relief of the flow is large enough compared with the thickness of the layer, the flow develops a relatively flat top and a steeply sloping front (e.g. M^cKenzie *et al.* 2000, their fig. 7), in agreement with the large-scale morphology of southern Tibet. In this situation the velocity at a given point on the surface of the current depends on the horizontal pressure gradient, the surface topography of the flow, the viscosity, and the density contrast between the flow and the substrate (which determines the thickness of the flow). The pressure gradient can be estimated from the topography at the Earth's surface, as can the topography on the surface of the flow if it is assumed that the brittle upper layer has an approximately constant thickness. We first isolate the long-wavelength topography of the plateau by low-pass filtering with radial Gaussian filters of diameters between 600 and 1200 km.

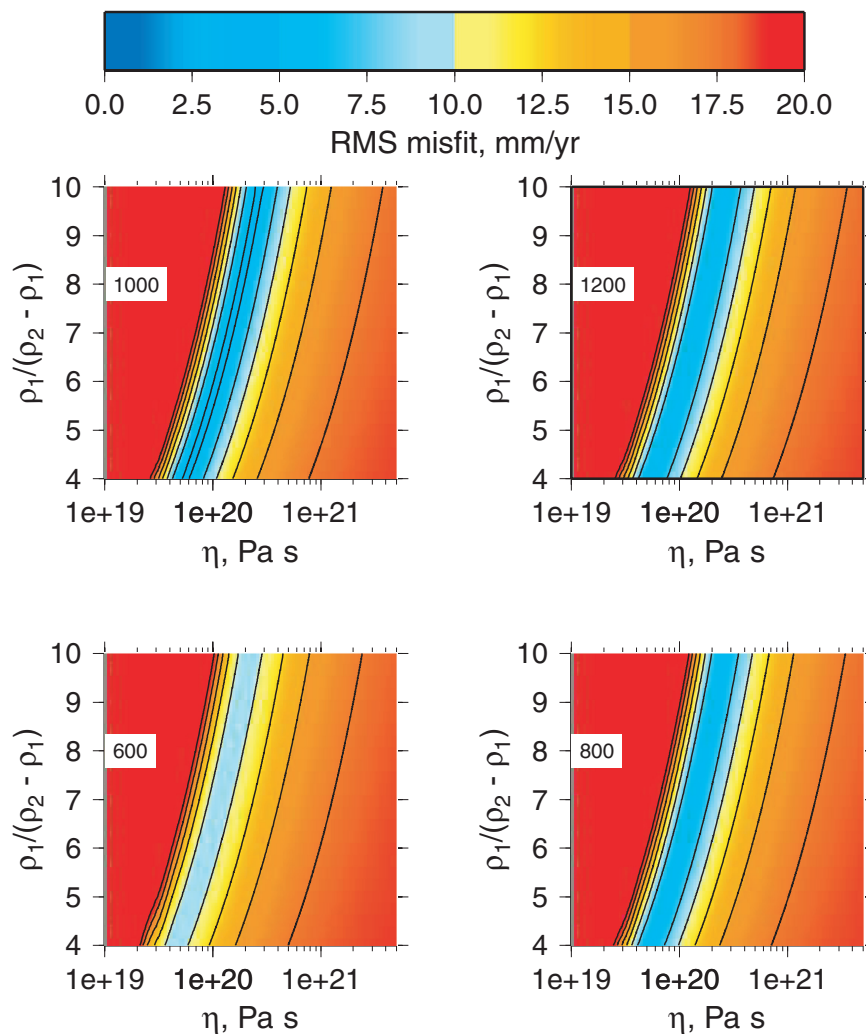


Figure 3. Plots of rms misfit (in mm yr^{-1}) between the model and GPS velocities for the sites shown in Fig. 2, as a function of density contrast (f) and viscosity (η). The numbers in the upper left corner of each plot represent the diameter (in km) of the Gaussian filter used to low-pass filter the topography. The contour interval is 2.5 mm yr^{-1} . Only contours of 20 mm yr^{-1} and below are shown.

We choose these filter diameters to remove the short-wavelength topography related to flexure and to preserve the long-wavelength topography (with wavelengths similar to the lengthscale of the flow we consider). As will be shown later, the choice of filter diameter has a limited effect on the results of our calculations (Fig. 3). We calculate the shear stresses on horizontal planes in this flow to be on the order of megapascals (calculated from the likely velocity gradients and our results for the viscosity of the flow). At these shear stresses diffusion (Newtonian) creep may be the dominant deformation mechanism in the ductile part of the crust, depending on which mineral phases govern the behaviour of the flow and the grain size of the minerals involved (see Section 6). Partly for this reason, and partly to simplify the mathematics involved, we use a Newtonian rheology. We calculate the surface velocities resulting from this flow using the equation

$$\mathbf{u} = -\frac{\rho_1 g (f + 1)^2}{2\eta} h^2 \nabla h \equiv A h^2 \nabla h \quad (1)$$

(McKenzie *et al.* 2000), where $\mathbf{u} = (u, v)$ is the surface velocity, η is the viscosity of the flowing layer, h is the elevation of the flow surface above the level of the ‘nose’ of the flow, and $f =$

$\rho_1 / (\rho_2 - \rho_1)$, where ρ_1 and ρ_2 are the densities of the flowing layer and the substrate, respectively.

We compare our calculated velocities to published GPS measurements. We use the velocities of Zhang *et al.* (2004) for stations in the southern plateau which are close enough to the plateau margins to be affected by the flow we are modelling, but far enough away from the margins (e.g. over $\sim 250 \text{ km}$) not to be affected by elastic deformation around the thrust faults on the plateau edges. To extend coverage westwards, we also use the stations LEH and MUTH of Jade *et al.* (2004) (the westernmost two velocities shown on Fig. 2). We use only these two stations because they are furthest from the surface trace of the Karakoram Fault, and so will be least affected by elastic strain accumulation. We convert Zhang *et al.*'s (2004) velocities relative to Eurasia and Jade *et al.*'s (2004) velocities in the ITRF97 reference frame to velocities relative to India using Sella *et al.*'s (2002) poles of relative rotation. Although errors will be introduced by these transformations, the GPS velocities will still be sufficiently accurate to allow us to test our simple model. An example of our calculated surface velocities, along with the published GPS velocities, are shown in Fig. 2. By minimizing the rms misfit between the model and GPS velocities we can determine the value of

the parameter A in eq. (1) to be $\sim 10^{-15} \text{ m}^{-1} \text{ s}^{-1}$. We cannot uniquely determine the viscosity, but the rms misfit between the model and GPS velocities, as a function of viscosity and the density contrast between the flowing layer and the substrate (and so the thickness of the flow), is shown in Fig. 3. It is not clear what densities should be used when deciding on the value of f . However, f can be estimated from the size of the surface relief and the depth of the top of the underthrust Indian lithosphere (~ 50 km in the northern part of the area we study (e.g. Owens & Zandt 1997)). The value of f is the factor which, if multiplied by the relief on the surface of the flow, gives the thickness of the corresponding 'root'. In the northern part of the area we have studied, towards the centre of the plateau, if the brittle upper crust is taken to be ~ 10 km thick, the flowing layer is ~ 40 km thick, of which ~ 5 km represents the relief on the upper surface. This means the thickness of the corresponding root is ~ 35 km, which gives a value of f of ~ 7 . For this value of f and

a viscosity of $\sim 2 \times 10^{20}$ Pa s there is good agreement between the model and GPS velocities. Other values of f give equally good agreement to the GPS data for different viscosities.

To summarize, the surface motions in southern Tibet can be described by the equation for isostatically compensated gravitationally driven flow over a rigid and deformable lower boundary. This result will be discussed in relation to other studies of this area in Section 7.

4 THE INDO-BURMAN RANGES

The Indo-Burman Ranges are an arcuate mountain belt along the northeastern margin of the Indian Shield (Fig. 1). Fig. 4 shows the seismicity of the Ranges and the surrounding areas. Coloured blue in (a) are the focal mechanisms of earthquakes in the CMT catalogue (with more than 70 per cent double couple, as defined

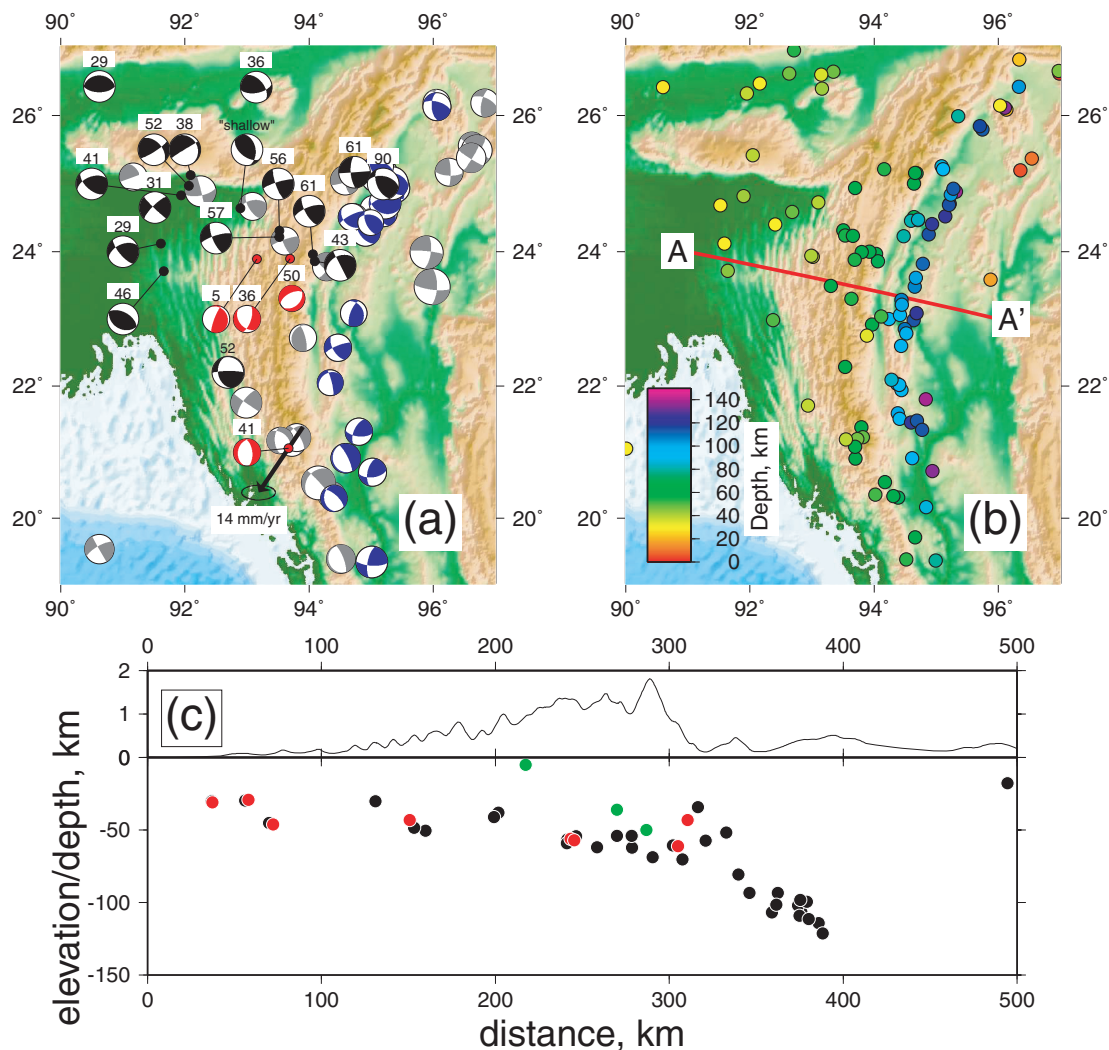


Figure 4. Topography and seismicity of the Indo-Burman ranges and surrounding areas. The area of coverage is shown by box b in Fig. 1. (a) Focal mechanisms shown in black are from Chen & Molnar (1990) and Mitra (2005), and are labelled with the depth in km. Those in red are from the CMT catalogue with depths determined in this study (Appendix A), and are also labelled with the depth. Those in grey are from the CMT catalogue, with more than 70 per cent double couple (as defined earlier) with depths in the Engdahl *et al.* (1998) catalogue of less than 70 km, and those in blue are from the same source but with depths in the Engdahl *et al.* (1998) catalogue of more than 70 km. Also shown (black arrow) is the velocity relative to India of the GPS station MIND (at $\sim 94^\circ\text{E}$ 21°N , Socquet *et al.* 2006). (b) Earthquakes from the Engdahl *et al.* (1998) catalogue with magnitudes greater than 5.0 and with more than 10 depth phase observations. The earthquakes are colour-coded for depth. (c) Cross-section along the line A–A' shown in (b). Note the different vertical scales for topography and earthquake depth. Black circles are earthquakes from the catalogue of Engdahl *et al.* (1998) shown in (b), red circles are from Chen & Molnar (1990) and Mitra (2005), and green circles are for earthquakes with depths determined by this study (Appendix A).

in the caption to Fig. 2) which have depths in the Engdahl *et al.* (1998) catalogue of more than 70 km. As can be seen in (c), these events all occur beneath the lowlands to the east of the Ranges, and occur at depths of up to ~150 km, showing subduction to be occurring beneath the lowlands. To the west of the Ranges, earthquakes occur at depths of up to ~50 km (which is unusually deep for the continents, e.g. Jackson 2002), and commonly have strike-slip mechanisms with N–NE oriented *P*-axes (Chen & Molnar 1990). Below the ranges themselves, the majority of the earthquakes which have well-determined depths (Chen & Molnar 1990; Mitra 2005, this paper Appendix A) occur at similar depths to those further west. This is a feature also shown by the earthquakes in the Engdahl *et al.* (1998) catalogue, shown in (b). Most of the earthquakes below the ranges are one of the following two types. First, numerous earthquakes have strike-slip mechanisms with N–NE oriented *P*-axes. The similarity between the depths and focal mechanisms of these earthquakes and those in Indian lithospheric material further west suggests that the Indian lithosphere underlies the Indo–Burman ranges at depth. The second commonly occurring type of earthquake below the ranges are normal-faulting earthquakes with N–NE oriented nodal planes. It is likely that these earthquakes occurred in response to tension in the Indian lithosphere caused by bending due to the downward pull of the subducting slab to the east, much like the normal faulting earthquakes often seen beneath the outer rises near subduction zones (Chapple & Forsyth 1979). Gowd *et al.* (1992) showed that the orientation of the maximum compressive stress in the Indo–Burman ranges (~E–W) is different from that in the central to northern Indian shield (~NE–SW), and from that in the underthrust Indian lithosphere (as suggested by N–NE oriented earthquake *P*-axes, Chen & Molnar 1990). The range-parallel trend of fold axes (e.g. Le Dain *et al.* 1984, and visible in the elevation data shown in Fig. 4) suggests that shortening occurs normal to the range throughout the mountain belt, regardless of local strike. This pattern is consistent with the observed velocity of the GPS station MIND (Socquet *et al.* 2006) which is approximately radial to the strike of the belt (see Fig. 4a), and with the mechanism of the earthquake which occurred at a depth of 5 km and is shown in red at ~93°E 24°N in Fig. 4, which presumably occurred on the low-angle nodal plane, and if so would have a slip vector approximately radial to the local strike of the range. The earthquake just to the north of this described as ‘shallow’ by Chen & Molnar (1990) (Fig. 4) may also have had a slip vector approximately radial to the range, depending on which nodal plane was the fault plane.

Deformed quaternary sediments (e.g. Le Dain *et al.* 1984), and the shallow thrusting earthquake just discussed show the deformation in the ranges to be currently active. Without significant ~N/S shortening of the Indian lithosphere, or ~N/S extension in the Indo–Burman Ranges themselves, for which there is no evidence, it is hard to see how the shortening can remain belt-perpendicular throughout the Indo–Burman Ranges if the deformation is the result of the relative motion of two rigid blocks. We suggest that the belt-perpendicular shortening throughout the length of the Indo–Burman Ranges is the result of gravitationally driven deformation in the ranges causing range-perpendicular flow over the underlying Indian lithosphere, in exactly the same way as we suggest southern Tibet overrides India (Section 3). We model this as the flow of a gravity current with a zero-horizontal-velocity base and a stress-free surface. We suggest that this deformation represents diffusion creep in the thick sequence of turbiditic shales and sandstones which form the ranges (Brunschweiler 1966; Mitchell 1981). Diffusion creep

(often referred to in the literature as pressure solution creep when water-assisted diffusive mass transfer is occurring over the scale of grains in sedimentary rocks) is known to occur in sediments at relatively low temperatures, and will result in a Newtonian rheology (e.g. Rutter 1983), so we model the deformation in this area as that of a Newtonian fluid. Shear-enhanced compaction and granular flow may also play a role in the deformation (e.g. Ngwenya *et al.* 2001), as might brittle failure. The lack of earthquakes within the Ranges (the seismicity being confined to the underlying Indian lithosphere and, in the case of the shallow thrust event mentioned above, the interface between the ranges and the underthrusting Indian material), supports the choice of a ductile rheology.

The Indo–Burman Ranges describe a small-circle on the Earth’s surface with a radius of approximately 500 km. Unlike the Tibetan Plateau, the surface velocities in the Indo–Burman Ranges are not well known. Therefore, rather than calculating a detailed velocity field, we make use of the axisymmetric nature of the ranges and calculate velocities from a profile produced by projecting the topography of the ranges onto a single plane. We then suggest what viscosities would produce the likely surface velocities.

The pole to the small-circle which approximates the Indo–Burman Ranges was calculated by finding the best-fitting small-circles to contours of elevation on the westward flank of the range (Fig. 1). The poles we have calculated using different contours vary in position by up ~60 km from the mean, but undertaking the following calculations using the extremes in the range of values does not appreciably change our results. The topography of the ranges was projected onto a single plane using the position of the pole and Fig. 5(a) shows how the topography varies with distance from the pole, along with the value of the topographic gradient.

We calculate the velocities which result from this combination of elevation and surface slope using two different geometries for the lower boundary. The first is an isostatically compensated lower boundary, in which case the velocity is given by eq. (1). The second geometry is that of a gently dipping lower boundary (dipping in the direction perpendicular to the flow front at all times), which will approximate the geometry expected for a gently flexed elastic layer. In this case the instantaneous velocity is given by

$$u_r = -\frac{\rho g}{\eta} \left\{ \frac{h^2}{2} + \frac{[(r_n - r)m]^2}{2} + hm(r_n - r) \right\} \frac{\partial h}{\partial r}, \quad (2)$$

where u_r is the radial velocity, r is the radial coordinate (with zero at the pole to which the ranges describe a small circle), m is the gradient of the lower boundary, r_n is the radial position of the ‘nose’ of the flow, and all other symbols have the same meanings as earlier. This equation is derived by following the method of Huppert (1982), but applying the lower boundary condition at a depth of $z = -(r_n - r)m$. We show the results of our calculations for lower boundaries with gradients of 0.05, 0.1 and 0.15, a range which covers the gradients compatible with the variation in depth of the earthquakes below the Ranges.

Fig. 5(c) shows how the maximum surface velocities for the two geometries of flow we have considered vary with the viscosity of the flow. The precise velocity of the flow is unknown. However, it probably lies in the range 1–20 mm yr⁻¹ (the GPS station MIND moves at ~14 mm yr⁻¹, Socquet *et al.* (2006), see Fig. 4), which would suggest a viscosity of ~2 × 10¹⁹–3 × 10²⁰ Pa s for an isostatically compensated flow, or one with a lower boundary with a gradient of 0.1. Lower boundaries with gradients of 0.05 and 0.15

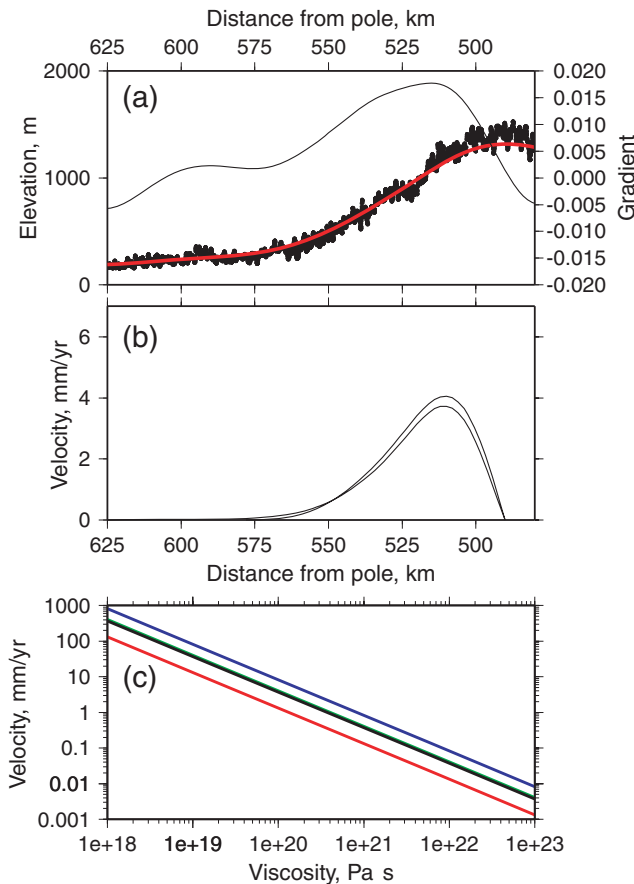


Figure 5. (a) The thick black line (actually a series of closely spaced points) shows the topography of the Indo–Burman Ranges as a function of distance from the pole to which the ranges describe a small circle. Each point represents the average of the topography of all the points in the range over a width of 1 km from the pole. The red line shows this topography after low-pass filtering. The thin black line shows the gradient of the filtered topography. (b) The surface velocities calculated using the topography and gradients shown in (a) for a gravity current propagating over a surface with a gradient of 0.1 (upper line) and an isostatically compensated gravity current (lower line), for a viscosity of 1×10^{20} Pa s. (c) The maximum surface velocity for a gravity current propagating over a lower boundary with a gradient of 0.05 (red), 0.1 (green, mostly obscured beneath the black) and 0.15 (blue), and an isostatically compensated gravity current (black), as a function of the viscosity of the flow.

give viscosity estimates of $\sim 6 \times 10^{19}$ – 1×10^{20} Pa s and $\sim 4 \times 10^{19}$ – 8×10^{20} Pa s, respectively. These estimates are similar to that of Nino *et al.* (1998), who suggest a viscosity of 10^{20} – 10^{21} Pa s for the thick sequence of Tertiary sandstones and shales in the Ventura Basin, California. Gratier *et al.* (1999) estimate a viscosity of 10^{21} Pa s for pressure solution creep in conglomerates, using a model involving both pressure solution creep and brittle fracturing. Connolly & Podladchikov (2000) estimate the viscosity in a sequence of shales and sandstones to be 10^{20} – 10^{21} Pa s, based on a viscoelastic model for sedimentary compaction. These estimates correspond to similar sediments at similar depths/thicknesses to those which we consider here, showing our estimate for the viscosity of the Indo–Burman Ranges to be generally consistent with other suggestions for sediments under similar conditions.

5 SOUTHEASTERN TIBETAN PLATEAU

GPS data (Zhang *et al.* 2004; Shen *et al.* 2005) show southeast-directed velocities (in the Eurasian and South China reference frames) on the southeastern margin of the Tibetan Plateau, in the area between the Szechwan basin and the Eastern Himalayan Syntaxis (Fig. 1). Fig. 6 shows the velocities we calculate for the area if the same model is used as for southern Tibet (Section 3). The large and spatially organized misfits between the GPS data and the model velocities show this model to be inappropriate for this area. We suggest that, rather than flow overriding a horizontally rigid substrate, the motion in this area may represent flow with a stress-free base confined between rigid walls (the Szechwan Basin and the lowlands near the Eastern Syntaxis), flowing in response to the topographic gradient parallel to the walls. We suggest a stress-free base in the absence of any information suggesting a rigid substrate in this area (such as the Indian lithosphere further west). This is the model which we will use for the remainder of this section.

The Szechwan basin and the lowlands near the Eastern Syntaxis (the ‘Central Lowlands’, Fig. 7a) are both characterized by low elevation and relief, suggesting that they have undergone less strain than the surrounding mountainous regions, and may represent relatively rigid areas. The Szechwan Basin is thought to be underlain by Precambrian crust (e.g. Burchfiel *et al.* 1995). The Central Lowlands are thought to be underlain by oceanic crust (e.g. Curray *et al.* 1978). Shen *et al.* (2005) show that the Szechwan basin is stationary in a south China reference frame. The motion of the northern part of the Central Lowlands is not known, but the decrease in velocities as the edge of the basin is approached in Fig. 7(a) suggests that it is moving slowly with respect to south China. We therefore model the velocities (relative to south China) in this area as the motion of a fluid between two parallel and stationary walls. Although the margins of the Szechwan Basin and the Central Lowlands are not perfectly parallel, this assumption simplifies the mathematics involved. As will be discussed later, it is likely that the flow in this area is directed southeastwards, rather than over the basins, because flow with a stress-free base is faster than flow limited by basal drag, as would be the case for flow over the basins. We make no assumptions regarding which layer of the lithosphere will be most viscous, and so likely to be governing the flow. The most viscous layer will, by definition, be underlain by material with a lower viscosity. We assume the viscosity contrast is large enough that the lower boundary can be approximated as stress-free.

Using the velocity gradients observed in the GPS data and our results for the viscosity of the flow (see below) we calculate that the horizontal shear stresses on vertical planes in this flow are on the order of tens of megapascals. At these shear stresses, the ductile part of the lithosphere will be deforming by dislocation (power-law) creep, rather than diffusion (Newtonian) creep (see Section 6). We therefore model the flow as that of a power-law fluid.

Using the geometry shown in Fig. B1, the velocity in the flow is given by (Appendix B)

$$u = \left(\frac{\sqrt{2}^{1/n-1}}{B} \frac{\partial P}{\partial x} \right)^n \left[\frac{y^{n+1} - (w/2)^{n+1}}{n+1} \right], \quad (3)$$

where w is the width of the flow, B and n are the rheological parameter and stress exponent from the constitutive equation for a power-law fluid (eq. B1), and $\partial P/\partial x$ is the pressure gradient in the x direction, which we have calculated from the topographic gradient as $\partial P/\partial x = \rho g \partial h/\partial x$, where ρ is density, g is the acceleration due to gravity, and h is elevation.

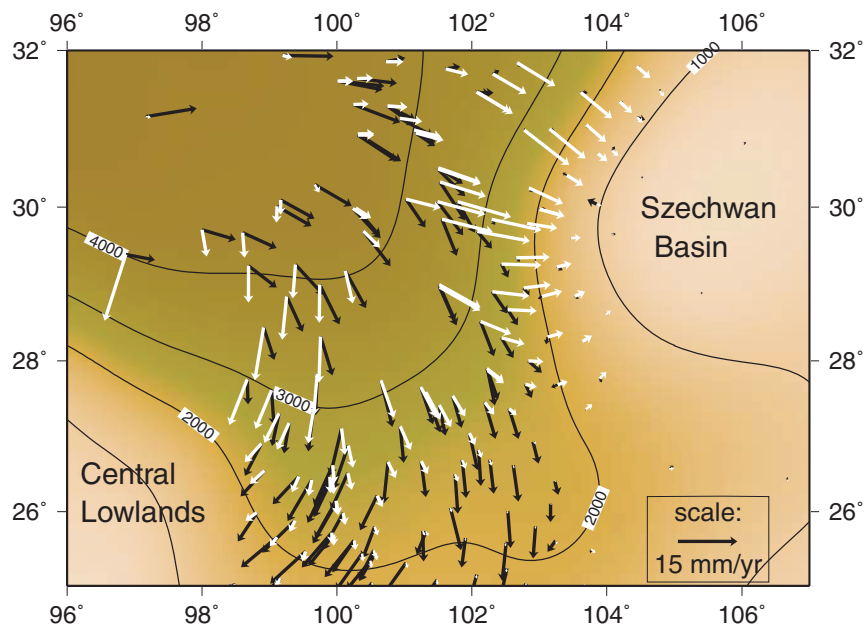


Figure 6. Long-wavelength topography of southeastern Tibet (created by low-pass filtering the topography using a radial Gaussian filter with a diameter of 500 km). Contours show the elevation in metres. Also pictured are GPS velocities (Shen *et al.* 2005) relative to south China (black). Error ellipses are omitted for clarity, but are small compared with the velocities (typically 1–2 mm yr⁻¹ at the 1 σ level). Shown in white are the velocities calculated using the model we used for southern Tibet (Section 3). The model velocities were calculated using a viscosity of 2×10^{20} Pa s, a value of f of 7, and using topography filtered with a Gaussian filter of diameter 500 km. Note the large and spatially organized misfits between the model and GPS velocities.

We find the values of B , n , and w which best fit a profile through the GPS measurements of Shen *et al.* (2005) (Fig. 7b). We find that a flow width of ~ 500 km gives the lowest rms misfits, a value which agrees well with the width of the area of elevated topography between the Szechwan basin and the Central Lowlands (Fig. 7b). B and n are related through the constitutive equation for a power-law fluid (eq. B1). We find that the rms misfit between the model and the GPS velocities is not significantly changed between values for n of 1 (Newtonian) and 5 (the maximum experimentally observed value of the stress-exponent in the dislocation creep of crustal and mantle minerals). The best-fitting value of B varies according to the value of n , but the effective viscosity of the lowest-misfit cases remains approximately constant at $\sim 1 \times 10^{22}$ Pa s. The rms misfit of these best-fitting combinations of parameters is less than 2 mm yr⁻¹ (Fig. 7c), which is approaching the accuracy of the GPS data.

To summarize, the surface motions in the area between the Szechwan Basin and the Eastern Syntaxis can be accurately described by an equation describing fluid flow between stationary walls in response to a horizontal pressure gradient.

6 DEFORMATION MAPS

In this section, we use experimental results (Boland & Tullis 1986; Bystricky & Mackwell 2001; Dimanov *et al.* 2003; Hirth & Kohlstedt 2003; Rybacki & Dresen 2004; Hier-Majumder *et al.* 2005, and references therein) to create deformation maps for the mineral phases likely to play an important role in crustal and mantle flow. We calculate strain-rates which can be used to plot contours of effective viscosity for a range of temperatures and differential stresses, and compare this rheological information for thermally activated creep to the results of the calculations described above.

Experimental results and theoretical considerations suggest flow laws (for a given mineral deforming by a given creep mechanism)

of the form

$$\dot{\epsilon} = A\sigma^n d^{-p} C_{OH}^r \exp\left(-\frac{E^* + PV^*}{RT}\right), \quad (4)$$

(e.g. Hirth & Kohlstedt 2003) where $\dot{\epsilon}$ is strain rate, A , p , and r are constants, σ is differential stress, n is a constant known as the stress exponent, d is grain size, C_{OH} is a measure of water content (sometimes replaced by a water fugacity term), E^* is the activation energy, V^* is the activation volume, P is pressure, T is temperature, and R is the gas constant. For diffusion creep, n equals 1, and the rheology is Newtonian. For dislocation creep, n is 3 or more, and the deformation is described as power-law creep. Using the values for the parameters in eq. (4) which have been experimentally determined, it is possible to extrapolate from the relatively small grain sizes and high strain-rates used in laboratory experiments to geological conditions. Effective viscosities can then be calculated using the values of stress and strain-rate. We calculated strain-rates for ‘wet’ and ‘dry’ conditions for olivine, diopside, and anorthite deforming in the diffusion creep and dislocation creep regimes at a range of differential stresses and temperatures, and grain sizes of 1 and 10 mm. For olivine we have used the values of parameters from Hirth & Kohlstedt (2003) and references therein. The experimental results for diopside and anorthite are from Boland & Tullis (1986); Bystricky & Mackwell (2001); Dimanov *et al.* (2003); Rybacki & Dresen (2004); Hier-Majumder *et al.* (2005), although these papers do not contain information regarding the activation volume and in some cases the water content/fugacity exponent. In these cases the ‘wet’ deformation maps represent extrapolations made using the water contents used in the experimental studies. The activation volume is likely to have a value of $\sim 10^{-5}$ m³ mol⁻¹ (e.g. Hirth & Kohlstedt 2003) and has little effect on the creep behaviour at the shallow depths with which we are concerned.

The calculations described above (Section 5) suggest that the effective viscosity of the flow in the area between the Szechwan Basin

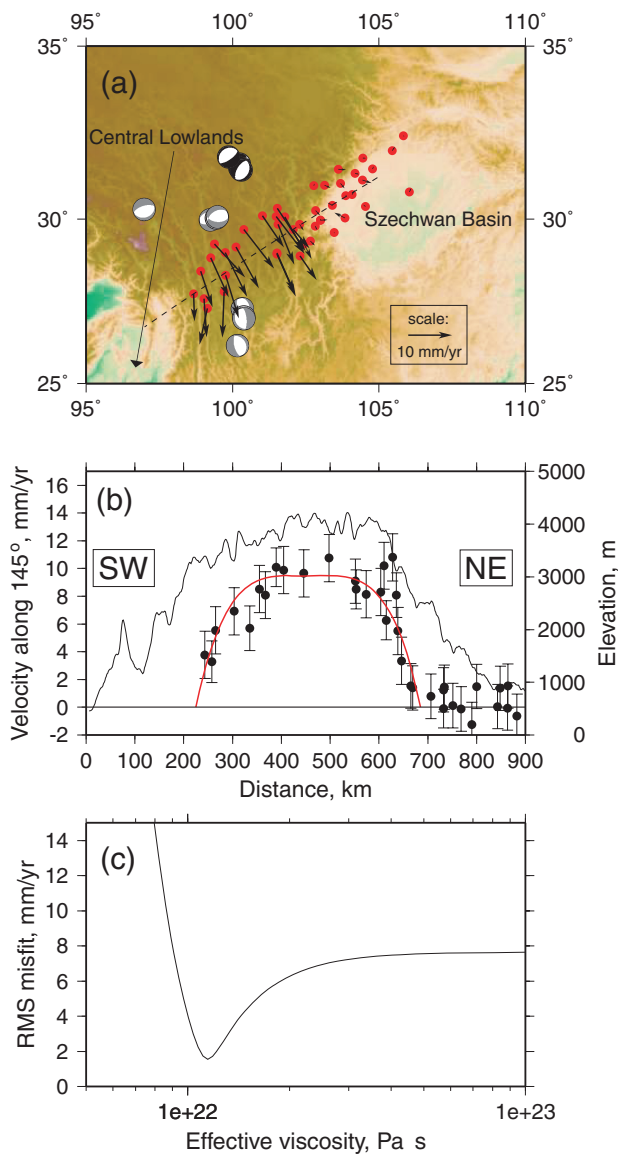


Figure 7. (a) Topography of the southeastern Tibetan Plateau. The area of coverage is shown by box c in Fig. 1. The red circles denote the locations of the GPS sites of Shen *et al.* (2005) which were used in modelling the flow. Error ellipses omitted for clarity. Velocities are in the South China reference frame. Also shown are normal faulting earthquakes which have occurred in the area (those shown in grey are from the CMT catalogue, with rakes within 30° of -90° and with more than 80 per cent double couple, and those shown in black are from Zhou *et al.* 1983). (b) The black line shows the topography along the line of the profile through the GPS data shown as the dashed line in (a). The black circles show the component of velocity in the direction 145° (down the topographic slope and parallel to the ‘walls’ of the flow). The error bars represent 1σ error estimates. The red line shows the best-fitting velocity profile from the model if the stress-exponent is set to 3. (c) rms misfit between the GPS velocities shown in (b) and the model, for a stress-exponent of 3, as a function of effective viscosity (calculated from the value of B in eq. (3) and a strain-rate of 10^{-15} s^{-1}). Only those GPS sites at locations which correspond to a distance of less than 700 km from the Central Lowlands in (b) were used to calculate the misfit.

and the Eastern Syntaxis is $\sim 10^{22} \text{ Pa s}$. Fig. 8 shows the $1 \times 10^{22} \text{ Pa s}$ viscosity contours for dry and wet olivine, diopside and anorthite deforming in the diffusion and dislocation creep regimes. At this viscosity and for shear stresses, and so differential stresses, of tens

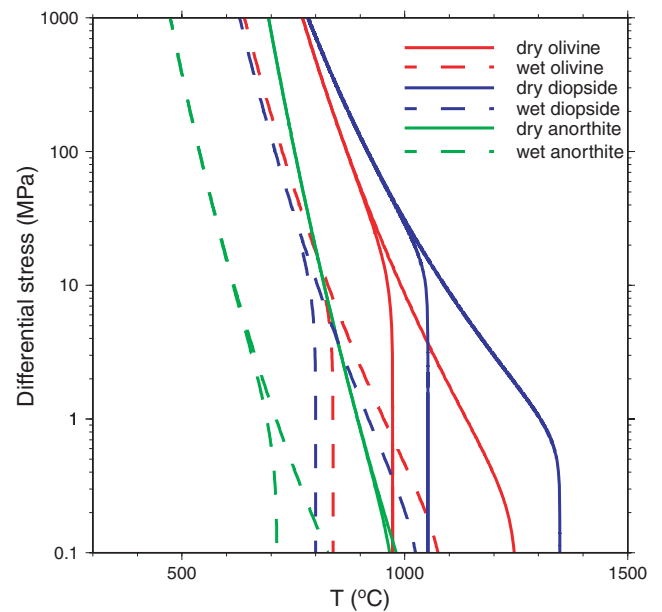


Figure 8. Contours of effective viscosity of 10^{22} Pa s for olivine (red), anorthite (green) and diopside (blue). There are two lines of each colour, the left hand (dashed) line represents deformation under ‘wet’ conditions, whilst the right hand (solid) line represents deformation under ‘dry’ conditions. Each line branches. The right hand branch represents a grain size of 10 mm, whilst the left hand branch represents a grain size of 1 mm. The sloping (higher stress) parts of the lines indicate deformation dominantly by dislocation (power-law) creep, the vertical parts of the lines indicate deformation dominantly by diffusion (Newtonian) creep.

of megapascals (Section 5), the minerals considered are likely to deform by dislocation creep (non-vertical lines on Fig. 8), supporting the choice of a power-law rheology for this flow. The experimentally determined values of the stress exponent vary between 3 (anorthite, Rybacki & Dresen 2004), 3.5 (olivine, Hirth & Kohlstedt 2003) and 5 (diopside, Dimanov *et al.* 2003). Modelling of the flow in the area between the Szechwan Basin and the Eastern Syntaxis does not provide any constraints on the value of the stress exponent in the flow, and therefore does not allow us to deduce which mineral species are governing the flow by comparison with experimentally deduced stress exponents. However, some inferences may be drawn based on information about the likely temperature structure in the area and the nature of the upper mantle. Hacker *et al.* (2000) obtained pressure–temperature estimates from crustal xenoliths in northern Tibet and suggest Moho temperatures of 1000°C or higher. Shu (1995) studied mantle xenoliths from southeast of the Plateau (at $104^\circ\text{E } 23^\circ\text{N}$) and found temperatures in the upper mantle of $\sim 1000^\circ\text{C}$. Wang *et al.* (2001) used crustal xenoliths to estimate the temperature at depths of $\sim 20\text{--}30 \text{ km}$ at $100^\circ\text{E } 26^\circ\text{N}$ to be $\sim 800^\circ\text{C}$, although this estimate is from xenoliths in rocks erupted at 42–24 Ma. McNamara *et al.* (1997) use seismological techniques to study the upper mantle below the Tibetan Plateau and obtain estimates of Moho temperature of $\sim 850\text{--}1200^\circ\text{C}$. At these upper mantle temperatures ‘dry’ olivine and diopside could have a viscosity of $\sim 1 \times 10^{22} \text{ Pa s}$, and ‘wet’ olivine and diopside would be considerably weaker. It has been suggested (Wang *et al.* 2001; Guo *et al.* 2005; Hou *et al.* 2006; Jiang *et al.* 2006) that southeastern Tibet is underlain by metasomatized lithospheric mantle enriched by subduction-derived fluids. It therefore seems more likely that the upper mantle in this area is ‘wet’ than ‘dry’, and therefore less viscous than the 10^{22} Pa s that we suggest for the flow in southeastern Tibet. Fig. 8 shows that the

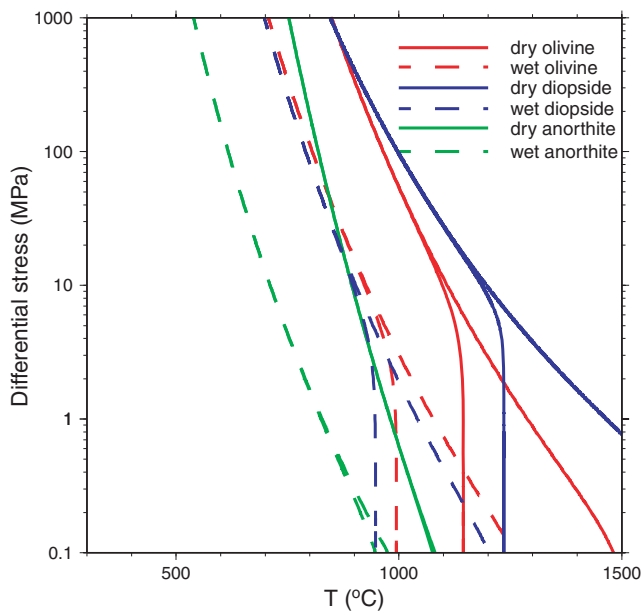


Figure 9. As Fig. 8, but for a viscosity of 10^{20} Pa s.

viscosity and stresses which we estimate for the flow are compatible with mineral deformation at mid to lower crustal temperatures.

In Section 3, we estimated the viscosity of the crust in southern Tibet to be $\sim 10^{20}$ Pa s. Fig. 9 shows the 1×10^{20} Pa s contours of effective viscosity for 'dry' and 'wet' olivine, diopside and anorthite. There are no estimates of the temperature in southern Tibet from xenoliths. However, pressure–temperature estimates from metamorphic rocks give an indication of the likely temperatures in the crust in southern Tibet. Lee *et al.* (2004) studied a southern Tibetan gneiss dome and suggested temperatures of $\sim 700^\circ\text{C}$ at pressures which correspond to depths of ~ 30 km. Harris *et al.* (2004) and Booth (2005) studied rocks exposed in the eastern Himalaya and suggested temperatures of 750°C and $700\text{--}900^\circ\text{C}$ at pressures corresponding to depths of ~ 30 km and $35\text{--}55$ km, respectively. Although these rocks record the pressures and temperatures experienced in the past, they give an indication of likely current temperatures. Mechie *et al.* (2004) studied the seismic signature of the $\alpha - \beta$ quartz transition and suggested a temperature of 800°C at a depth of 32 km at $30\text{--}31^\circ\text{N}$, in the area likely to be underlain by Indian crustal material. The depth to the top of the strong Indian lithospheric material underlying the southern plateau is thought to be ~ 50 km (e.g. Owens & Zandt 1997), so in view of the above temperature estimates it seems likely that temperatures in excess of 800°C are present in the crust overlying the Indian lithospheric material. Fig. 9 suggests that wet or dry anorthite, and wet diopside and olivine would be expected to creep with an effective viscosity of $\sim 10^{20}$ Pa s at such temperatures and shear stresses (and so differential stresses) on the order of megapascals (Section 3). However, numerous studies (e.g. Makovsky *et al.* 1996; Li *et al.* 2003; Unsworth *et al.* 2005) have suggested the presence of aqueous fluids or partial melt in the crust of southern Tibet, which would reduce the applicability of Fig. 9, which assumes no fluid phases are present. The presence of aqueous fluids or partial melt would have the effect of moving a given viscosity contour to lower temperatures. Rosenberg & Handy (2005) suggest an abrupt reduction in the strength of granite of between one and two orders of magnitude at melt fractions of about 0.07. If a fluid phase is present in southern Tibet (Unsworth *et al.* 2005 suggest melt fractions in the mid-crust

of 0.05–0.14), the minerals mentioned above will be expected to deform with an effective viscosity of $\sim 10^{20}$ Pa s at lower temperatures than suggested by Fig. 9, although these temperatures will still be within the range suggested for the middle crust in this area.

7 DISCUSSION

We have used models of fluid flow in response to topographically produced horizontal pressure gradients to calculate surface velocities for parts of the India–Asia collision zone. For southern Tibet we have used a model with a rigid lower boundary (corresponding to Indian lithospheric material) and a stress free upper boundary, both of which can deform vertically. In this model flow is always down the topographic gradient, deformation is by simple shear on horizontal planes, and a steep topographic front forms at the nose of the flow. Velocities calculated from this model resemble the surface velocities in southern Tibet. If this model is used in southeastern Tibet (in the area between the Szechwan Basin and the Eastern Syntaxis), the calculated velocities do not resemble the GPS velocities. However, if the model has a stress-free base, and is confined between stationary walls, then the calculated velocities match the GPS measurements. This change in lower boundary condition may explain why there is no steep topographic front perpendicular to the flow direction in this area, as there is on the southern and southwestern margins of the plateau, and which is characteristic of a gravity current with a rigid lower boundary (e.g. McKenzie *et al.* 2000, their fig. 7). Although we have used simple models, the agreement between our calculations and the GPS measurements suggests that deformation in these parts of the India–Asia collision zone is the result of crustal flow in response to horizontal pressure gradients.

Other authors have also suggested that gravity-driven crustal flow can account for the deformation of the Tibetan Plateau. Royden (1996) and Shen *et al.* (2001) studied the evolution of the plateau through time. Their model included flow in the underthrust Indian crust, which we have suggested provides a rigid and deformable lower boundary to the flow occurring in the overriding material. Because of this they obtain a different value for the viscosity of the crust in southern Tibet ($0.5\text{--}3 \times 10^{21}$ Pa s). In addition, the topographic front that their flow develops has a gentle onset rather than a sharp front, presumably because, if the Indian crust is allowed to flow, the surface relief is not large enough compared with the flow thickness to produce a steep front (e.g. fig. 7 of McKenzie *et al.* 2000). Clark & Royden (2000) obtained viscosity estimates for flow in a fixed-width lower crustal channel of 10^{21} Pa s below the northern and southern margins of the plateau and 10^{18} Pa s beneath the lower gradient margins of the eastern plateau. They use rigid upper and lower boundaries and remove material from their flow after every timestep, placing it above and below the top and bottom of the fixed-width channel. In our model we use a stress-free upper boundary and allow the thickness of the flow to change. England & Molnar (1997) used a velocity field calculated from quaternary slip rates on faults, and a 'thin viscous sheet' model to estimate the effective viscosity of the Tibetan lithosphere to be 10^{22} Pa s. Flesch *et al.* (2001) studied gravity-driven deformation in the India–Asia collision zone, and obtained an estimate of effective viscosity of $0.5\text{--}5 \times 10^{22}$ Pa s for the Tibetan plateau. These models both use stress-free upper and lower boundary conditions, instead of a rigid lower boundary for southern Tibet as we use here. We do, however, also use stress-free upper and lower boundary conditions in the area between the Szechwan Basin and the Eastern Syntaxis, but unlike the other models we impose rigid lateral boundaries on the flow. Despite

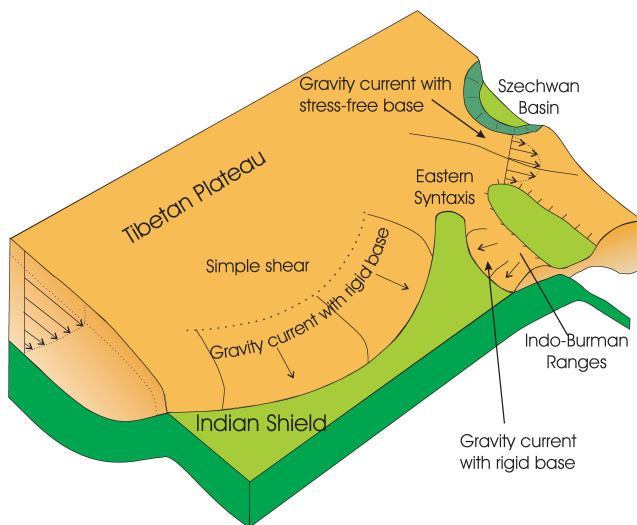


Figure 10. Cartoon to illustrate the deformation we model in the India–Asia collision zone.

these differences our viscosity estimate for this area is similar to the above estimates, namely 10^{22} Pa s.

Some features of the velocity field, however, do not match our model. GPS sites in the central plateau (those closest to the 5000 m contour in Fig. 2) show velocities relative to India which are directed perpendicular to the strike of the topographic front, as are those closer to the plateau margin which we model as a gravity current in Section 3. In our model the velocities at these locations in the central plateau are negligible (due to the low values of the surface gradient). If underthrust Indian lithosphere extends as far as $\sim 33^\circ\text{N}$ (e.g. DeCelles *et al.* 2002; Tilmann *et al.* 2003), then the locations of these GPS sites, along with large areas of the central plateau, are underlain by Indian material. Along with the GPS measurements, this means the middle crust in the area may be deforming by simple shear on horizontal planes (Fig. 10). This shear could be driven by stress transmission through horizontal layers, such as the brittle upper crust. In this situation, simple shear in central Tibet is driven by the southwards motion of Eurasia. Alternatively, if the underthrust Indian lithosphere does not extend this far from the plateau margin, a stress-free lower boundary condition may be appropriate for the central plateau, in which case stresses which we have not taken into account in our modelling (e.g. deviatoric stresses normal to vertical planes) will be important, and may drive the motions in central Tibet.

Large misfits between the geodetically determined velocities and our model velocities occur for the furthest east and west GPS stations in Fig. 2. These misfits may result from our method of isolating the long wavelength topography, as both stations are close to the edges of the area where the Himalayan front forms a smooth arc, and close to where the shape of the topography undergoes more abrupt changes (and also, in the case of the furthest east station, where the topographic slope at the northern margin of the plateau begins to influence the shape of the smoothed topography). Alternatively, the stations are also the closest to the eastern and western limits of the area that is likely to be underlain by Indian lithospheric material, so the crust here may well be experiencing forces which are not taken into account in our simple model.

We have suggested that the lower boundary condition changes between southern Tibet (rigid and deformable) and the area between the Szechwan Basin and the Eastern Syntaxis (stress-free). This situation is analogous to that of ice sheets and ice streams (e.g. MacAyeal

1989). The motion of ice sheets is governed by basal drag, the base of the ice being frozen to the substrate. In fast-moving ice-streams, however, the bed is thought to be lubricated, or to overlie easily deformable sediments (e.g. Blankenship *et al.* 1987), so the main drag is from the edges of the stream, and the ice flows significantly faster than in the interiors of ice sheets. Even though we calculate the effective viscosity to be two orders of magnitude higher in the area between the Szechwan Basin and the Eastern Syntaxis than in southern Tibet, the surface velocities are of a similar magnitude. In Section 5, we suggested that the flow in the area between the Eastern Syntaxis and the Szechwan Basin has a stress-free base, and so is flowing in a manner analogous to an ice stream, whilst in southern Tibet the flow is limited by basal drag, as with ice sheets. It is likely that the flow of material in the area between the Eastern Syntaxis and the Szechwan Basin is directed to the southeast, rather than perpendicular to this in the direction of the greatest topographic gradient (over the adjacent lowlands), because flow southeastwards with a stress-free base occurs faster than flow over the basins limited by basal drag.

One of the more notable geomorphological features in southeastern Tibet is the proximity of three large rivers flowing southeastwards (the Salween, Mekong and Yangtze rivers). Hallet & Molnar (2001) suggested these river valleys record the finite deformation of the underlying crust. They suggest the proximity of the rivers is due to NE–SW shortening, and dextral shear along a north trending zone, caused by the northwards motion of India relative to Eurasia. Another possibility is that the river valleys may be closely spaced because of the flow we describe between the Szechwan Basin and the Eastern Syntaxis. As material flows into this area, the SSE-wards velocity increases. This will lead to contraction in the direction perpendicular to the flow direction, which would result in decreasing the distance between the river valleys. In this sense, the large river valleys may be viewed in a similar manner to glacial moraines, recording the flow of the underlying material.

Fig. 2 shows that the majority of the normal faulting earthquakes in the Tibetan Plateau occur near the southern margin, in the area where we model the surface velocities as viscous flow over the Indian Shield. This suggests that the majority of the normal faulting earthquakes currently occurring within the plateau are caused by the gravitational spreading of Tibetan material over India, rather than occurring in response to increased gravitational potential energy after convective removal of the mantle lithosphere (e.g. Molnar *et al.* 1993).

Some normal faulting earthquakes have occurred near the Szechwan Basin and the Eastern Syntaxis (Fig. 7a). The earthquakes at latitudes of $\sim 30^\circ\text{N}$ have $\sim\text{E–W}$ fault planes. Immediately south of these earthquakes (in the area of the profile through the velocities shown in Fig. 7b) the surface gradient in the direction of the flow increases. We have shown that the flow in this area can be driven by the pressure gradient resulting from the surface slope, so we would expect a steeper gradient to result in larger downslope velocities than further north. This velocity difference would result in extension in the downslope direction at the northernmost margin of the steepening of slope, which is where the normal faulting earthquakes with the $\sim\text{E–W}$ fault planes have occurred. It therefore seems likely that earthquakes in this region are caused by the change in velocity due to the change in slope. Normal faulting earthquakes have also occurred further south, at $\sim 27^\circ\text{N}$. These earthquakes have $\sim\text{N–S}$ fault planes. These earthquakes have occurred just south of the latitude of the southern margin of the Szechwan Basin. South of the Szechwan Basin we would expect the flow of material to spread outwards, with a component of velocity perpendicular to the flow

direction further north, and down the topographic slope to the east. We would also expect increased westwards motion on the western margin of the flow, because the margin of the lowlands bounding the flow curves to the southwest in this area. These two effects would result in extension perpendicular to the bulk flow direction, and in the brittle upper crust would result in normal faulting with ~N–S fault planes, as with the earthquakes. Further work, with more detailed modelling, is needed to confirm these suggestions.

The lowlands near the Eastern Syntaxis have a distinctive shape. An elongate area with low relief and low elevation lies between the eastern Himalaya and the Indo–Burman Ranges, and is seemingly being overthrust on three sides. This geometry is not compatible with the motions of rigid blocks, given what we know about the tectonics of this area. The work presented in Sections 3 and 4 gives an alternative explanation for the formation of such syntaxes. Both southern Tibet and the Indo–Burman ranges are gravity currents propagating over the Indian shield, with motion down the topographic gradients, so normal to the strike of the fronts of the two mountain ranges. These two gravity currents are flowing towards each other in the area of the Eastern Syntaxis, both overriding the lowlands mentioned above, creating the distinctive geometry (Fig. 10). Syntaxes elsewhere (e.g. the western Himalayan Syntaxis) may also have formed in this manner.

8 CONCLUSIONS

We have modelled the measured surface velocities in parts of the India–Asia collision zone using equations describing fluid flow, and suggest that the motions in these areas are governed by gravitationally driven crustal flow. The viscosity of the material in southern Tibet is $\sim 10^{20}$ Pa s, and in the area between the Szechwan Basin and the Eastern Syntaxis it is $\sim 10^{22}$ Pa s. We suggest that the lower boundary condition changes between these two areas, from horizontally rigid and vertically deformable where strong Indian lithospheric material underlies southern Tibet, to stress-free in the area between the Szechwan Basin and the Eastern Syntaxis. We have used deformation maps, created using results from experimental studies, to show that the shear stresses, temperatures, and viscosities present in the flows we suggest are consistent with the available information on the rheology of minerals. Gravitationally driven flow also occurs in the Indo–Burman Ranges, with an effective viscosity of $\sim 10^{19}$ – 10^{20} Pa s. We suggest that the normal faulting earthquakes in southern Tibet (which account for most of the normal faulting earthquakes on the plateau) are caused by the gravity-driven spreading of Tibet southwards over the Indian shield.

ACKNOWLEDGMENTS

We thank L. Royden and an anonymous reviewer for helpful comments. The authors wish to thank James Jackson for many useful discussions and comments on the manuscript. Some figures were created using the Generic Mapping Tools (GMT) software (Wessel & Smith 1995).

REFERENCES

- Baranowski, J., Armbruster, J., Seeber, L. & Molnar, P., 1984. Focal depths and fault plane solutions of earthquakes and active tectonics of the Himalayas, *J. geophys. Res.*, **89**, 6918–6928.
- Beaumont, C., Jamieson, R.A., Nguyen, M.H. & Lee, B., 2001. Himalayan tectonics explained by extrusion of a low-viscosity crustal channel coupled to focused surface denudation, *Nature*, **141**, 738–742.
- Bird, P., 1991. Lateral extrusion of lower crust from under high topography, in the isostatic limit, *J. geophys. Res.*, **96**, 10 275–10 286.
- Blankenship, D.D., Bentley, C.R., Rooney, S.T. & Alley, R.B., 1987. Till beneath ice stream B, 1, Properties derived from seismic travel times, *J. geophys. Res.*, **92**, 8903–8911.
- Block, L. & Royden, L.H., 1990. Core complex geometries and regional scale flow in the lower crust, *Tectonics*, **9**, 557–567.
- Boland, J.N. & Tullis, T.E., 1986. Deformation behaviour of wet and dry clinopyroxene in the brittle to ductile transition region, in *Mineral and Rock Deformation: Laboratory Studies, Geophysical Monograph*, Vol. 36, pp. 35–49, eds Hobbs, B.E. & Heard, H.C., AGU, Washington.
- Booth, A.L., 2005. Pressure-temperature conditions and timing of metamorphism at Namche Barwa, Eastern Himalayan Syntaxis, SE Tibet, *Geological Society of America Abstracts with Programs*, **37**, 89.
- Brunnschweiler, R.O., 1966. On the geology of the Indoburman Ranges, *J. Geol. Soc. Aust.*, **13**, 137–194.
- Burchfiel, B.C., Chen, Z., Liu, Y. & Royden, L.H., 1995. Tectonics of the Longmen Shan and adjacent regions, central China, *Int. Geol. Rev.*, **37**, 661–735.
- Bystricky, M. & Mackwell, S., 2001. Creep of dry clinopyroxene aggregates, *J. geophys. Res.*, **106**, 13 443–13 454.
- Chapman, C.H., 1978. A new method for computing synthetic seismograms, *Geophys. J. R. astr. Soc.*, **54**, 481–518.
- Chapple, W.M. & Forsyth, D.W., 1979. Earthquakes and the bending of plates at trenches, *J. geophys. Res.*, **84**, 6729–6749.
- Chen, W.-P. & Kao, H., 1996. Seismotectonics of Asia: some recent progress, in *The Tectonic Evolution of Asia*, pp. 37–62, eds Yin, A. & Harrison, M., Cambridge University Press, Cambridge.
- Chen, W.-P. & Molnar, P., 1990. Source parameters of earthquakes and intraplate deformation beneath the Shillong Plateau and the northern Indoburman ranges, *J. geophys. Res.*, **95**, 12 527–12 552.
- Clark, M.K. & Royden, L.H., 2000. Topographic ooze: building the eastern margin of Tibet by lower crustal flow, *Geology*, **28**, 703–706.
- Clark, M.K., Bush, J.M.W. & Royden, L.H., 2005. Dynamic topography produced by lower crustal flow against rheological strength heterogeneities bordering the Tibetan Plateau, *Geophys. J. Int.*, **162**, 575–590.
- Connolly, J.A.D. & Podladchikov, Yu. Yu., 2000. Temperature-dependent viscoelastic compaction and compartmentalization in sedimentary basins, *Tectonophysics*, **324**, 137–168.
- Curry, J.R., Moore, D.G., Lawver, L.A., Emmel, F.J., Raitt, R.W., Henry, M. & Kieckhefer, R., 1978. Tectonics of the Andaman Sea and Burma. in *Geological and Geophysical Investigations of Continental Margins, Mem. Am. Assoc. Pet. Geol.*, Vol. 29, pp. 189–198, eds Watkins, J.S., Montadert, L. & Dickerson, P., AAPG, Tulsa.
- DeCelles, P., Robinson, D. & Zandt, G., 2002. Implications of shortening in the Himalayan fold-thrust belt for uplift of the Tibetan plateau, *Tectonics*, **21**, doi:10.1029/2001TC001322.
- Dimanov, A., Lavie, M.P., Dresen, G., Ingrin, J. & Jaoul, O., 2003. Creep of polycrystalline anorthite and diopside, *J. geophys. Res.*, **108**, doi:10.1029/2002JB001815.
- Engdahl, E.R., van der Hilst, R. & Buland, R., 1998. Global teleseismic earthquake relocation with improved travel times and procedures for depth determination, *Bull. seism. Soc. Am.*, **88**, 722–743.
- England, P. & Houseman, G., 1986. Finite strain calculations of continental deformation 2. Comparison with the India–Asia collision zone, *J. geophys. Res.*, **91**, 3664–3676.
- England, P. & McKenzie, D., 1982. A thin viscous sheet model for continental deformation, *Geophys. J. R. astr. Soc.*, **70**, 295–321.
- England, P. & Molnar, P., 1997. Active deformation of Asia: from kinematics to dynamics, *Science*, **278**, 647–650.
- Fielding, E.J., Isacks, B., Barazangi, M. & Duncan, C., 1994. How flat is Tibet?, *Geology*, **22**, 163–167.
- Flesch, L.M., Haines, A.J. & Holt, W.E., 2001. Dynamics of the India–Eurasia collision zone, *J. geophys. Res.*, **106**, 16 435–16 460.

- Gowd, T.N., Srirama Rao, S.V. & Gaur, V.K., 1992. Tectonic stress field in the Indian subcontinent, *J. geophys. Res.*, **97**, 11 879–11 888.
- Gratier, J.-P., Renard, F. & Labaume, P., 1999. How pressure solution creep and fracturing processes interact in the upper crust to make it behave in both a brittle and viscous manner, *J. Struct. Geol.*, **21**, 1189–1197.
- Guo, Z., Hertogen, J., Liu, J., Pasteels, P., Boven, A., Punzalan, L., He, H., Luo, X. & Zhang, W., 2005. Potassic magmatism in western Sichuan and Yunnan provinces, SE Tibet, China: petrological and geochemical constraints on petrogenesis, *J. Petrol.*, **46**, 33–78.
- Hacker, B.R., Gnos, E., Ratschbacher, L., Grove, M., McWilliams, M., Sobolev, S.V., Wan, J. & Zhenhan, W., 2000. Hot and dry deep crustal xenoliths from Tibet, *Science*, **287**, 2463–2466.
- Hallet, B. & Molnar, P., 2001. Distorted drainage basins as markers of crustal strain east of the Himalaya, *J. geophys. Res.*, **106**, 13 697–13 709.
- Harris, N.B.W., Caddick, M., Kosler, J., Goswami, S., Vance, D. & Tindle, A.G., 2004. The pressure-temperature-time path of migmatites from the Sikkim Himalaya, *J. metamorphic Geol.*, **22**, 249–264.
- Hier-Majumder, S., Mei, S. & Kohlstedt, D.L., 2005. Water weakening of clinopyroxene in diffusion creep, *J. geophys. Res.*, **110**, doi:10.1029/2004JB003414.
- Hirth, G. & Kohlstedt, D.L., 2003. Rheology of the upper mantle and the mantle wedge: a view from the experimentalists, in *Inside the Subduction Factory. Geophysical Monograph*, Vol. 138, pp. 83–105, ed. Eiler, J., American Geophysical Union.
- Hoke, L., Lamb, S., Hilton, D.R. & Poreda, R.J., 2000. Southern limit of mantle-derived geothermal helium emissions in Tibet: implications for lithospheric structure, *Earth planet. Sci. Lett.*, **180**, 297–308.
- Holt, W.E., Chamot-Rooke, N., Le Pichon, X., Haines, A.J., Shen-Tu, B. & Ren, J., 2000. Velocity field in Asia inferred from Quaternary fault slip rates and Global Positioning System observations, *J. geophys. Res.*, **105**, 19 185–19 209.
- Hou, Z., Tian, S., Yuan, Z., Xie, Y., Yin, S., Yi, L., Fei, H. & Yang, Z., 2006. The Himalayan collision zone carbonatites in western Sichuan, SW China: petrogenesis, mantle source and tectonic implication, *Earth planet. Sci. Lett.*, **244**, 234–250.
- Huang, W.-C. *et al.*, 2000. Seismic polarization anisotropy beneath the central Tibetan Plateau, *J. geophys. Res.*, **105**, 27 979–27 990.
- Huppert, H.E., 1982. The propagation of two-dimensional and axisymmetric gravity currents over a rigid horizontal surface, *J. Fluid Mech.*, **121**, 43–58.
- Jackson, J., Priestley, K., Allen, M. & Berberian, M., 2002. Active tectonics of the South Caspian Basin, *Geophys. J. Int.*, **148**, 214–245.
- Jackson, J.A., 2002. Strength of the continental lithosphere: time to abandon the jelly sandwich? *GSA Today*, **12**, 4–10.
- Jade, S., Bhatt, B.C., Yang, Z., Bendick, R., Gaur, V.K., Molnar, P., Anand, M.B. & Kumar, D., 2004. GPS measurements from the Ladakh Himalaya, India: Preliminary tests of plate-like or continuous deformation in Tibet, *GSA Bull.*, **116**, 1385–1391.
- Jiang, Y.-H., Jiang, S.-Y., Ling, H.-F. & Dai, B.-Z., 2006. Low-degree melting of a metasomatized lithospheric mantle for the origin of Cenozoic Yulong monzogranite-porphry, east Tibet: geochemical and Sr-Nd-Pb-Hf isotopic constraints, *Earth planet. Sci. Lett.*, **241**, 617–633.
- Jin, Y., McNutt, M.K. & Zhu, Y., 1996. Mapping the descent of the Indian and Eurasian plates beneath the Tibetan Plateau from gravity anomalies, *J. geophys. Res.*, **101**, 11 275–11 290.
- Kennett, B.L.N., Engdahl, E.R. & Buland, R., 1995. Constraints on seismic velocities in the Earth from travel times, *Geophys. J. R. astr. Soc.*, **122**, 108–124.
- Kruse, S., McNutt, M., Phipps-Morgan, J., Royden, L. & Wernicke, B., 1991. Lithospheric extension near Lake Mead, Nevada: a model for ductile flow in the lower crust, *J. geophys. Res.*, **96**, 4435–4456.
- Le Dain, A.Y., Tapponnier, P. & Molnar, P., 1984. Active faulting and tectonics of Burma and surrounding regions, *J. geophys. Res.*, **89**, 453–472.
- Lee, J., Hacker, B. & Wang, Y., 2004. Evolution of North Himalayan gneiss domes: structural and metamorphic studies in Mabja Dome, southern Tibet, *J. Struct. Geol.*, **26**, 2297–2316.
- Li, S., Unsworth, M.J., Booker, J.R., Wei, W., Tan, H. & Jones, A.G., 2003. Partial melt or aqueous fluid in the mid-crust of Southern Tibet? Constraints from INDEPTH magnetotelluric data, *Geophys. J. Int.*, **153**, 289–304.
- MacAyeal, D., 1989. Large-scale flow over a viscous basal sediment: theory and application to Ice Stream B, Antarctica, *J. geophys. Res.*, **94**, 4071–4087.
- Makovsky, Y., Klempner, S.L., Ratschbacher, L., Brown, L.D., Li, M., Zhao, W. & Mang, F., 1996. INDEPTH wide-angle reflection observation of P-wave-to-S-wave conversion from crustal bright spots in Tibet, *Science*, **274**, 1690–1691.
- McKenzie, D., Nimmo, F., Jackson, J., Gans, P.B. & Miller, E.L., 2000. Characteristics and consequences of flow in the lower crust, *J. geophys. Res.*, **105**, 11 029–11 046.
- McKenzie, D.P. & Fairhead, D., 1997. Estimates of the effective elastic thickness of the continental lithosphere from bouguer and free air gravity anomalies, *J. geophys. Res.*, **102**, 27 523–27 552.
- McNamara, D.E., Walter, W.R., Owens, T.J. & Ammon, C.J., 1997. Upper mantle velocity structure beneath the Tibetan Plateau from Pn travel time tomography, *J. geophys. Res.*, **102**, 10.1029/96JB02112..
- Mechie, J. *et al.*, 2004. Precise temperature estimation in the Tibetan crust from seismic detection of the $\alpha - \beta$ quartz transition, *Geology*, **32**, 601–604.
- Mitchell, A.H.G., 1981. Phanerozoic plate boundaries in mainland SE Asia, the Himalayas and Tibet, *J. Geol. Soc. Lond.*, **138**, 109–122.
- Mitra, S., 2005. Crustal structure and earthquake focal depths beneath north-eastern India and southern Tibet, *Geophys. J. Int.*, **160**, 227–248.
- Molnar, P. & Chen, W.-P., 1983. Focal depths and fault plane solutions of earthquakes under the Tibetan plateau, *J. geophys. Res.*, **88**, 1180–1196.
- Molnar, P. & Lyon-Caen, H., 1989. Fault plane solutions of earthquakes and active tectonics of the Tibetan plateau and its margins, *Geophys. J. Int.*, **99**, 123–153.
- Molnar, P., Chen, W.-P., Fitch, T.J., Tapponnier, P., Warsi, W.E.K. & Wu, F., 1977. Structure and tectonics of the Himalaya: a brief summary of relevant geophysical observations, in *Colloque Internationaux du CNRS, No 268, Himalaya: Sciences de la Terre*, Editions du Centre Nationale de la Recherche Scientifique, Paris, pp. 269–294.
- Molnar, P., England, P. & Martinod, J., 1993. Mantle dynamics, uplift of the Tibetan plateau, and the Indian monsoon, *Rev. Geophys.*, **31**, 357–396.
- Ngwenya, B.T., Main, I.G., Elphick, S.C., Crawford, B.R. & Smart, B.G.D., 2001. A constitutive law for low-temperature creep of water-saturated sandstones, *J. geophys. Res.*, **106**, 21 811–21 826.
- Nino, F., Chery, J. & Gratier, J.P., 1998. Mechanical modelling of compressional basins: origin and interaction of faults, erosion and subsidence, in the Ventura basin, California, *Tectonics*, **17**, 955–972.
- Owens, T. & Zandt, G., 1997. Implications of crustal property variations for models of Tibetan plateau evolution, *Nature*, **387**, 23–25.
- Rosenberg, C.L. & Handy, M.R., 2005. Experimental deformation of partially melted granite revisited: implications for the continental crust, *J. Metamorphic Geol.*, **23**, 19–28.
- Royden, L., 1996. Coupling and decoupling of crust and mantle in convergent orogens: Implications for strain partitioning in the crust, *J. geophys. Res.*, **101**, 17 679–17 705.
- Rutter, E.H., 1983. Pressure solution in nature, theory and experiment, *J. Geol. Soc. Lond.*, **140**, 725–740.
- Rybacki, E. & Dresen, G., 2004. Deformation mechanism maps for feldspar rocks, *Tectonophysics*, **382**, 173–187.
- Sella, G., Dixon, T. & Mao, A., 2002. REVEL: a model for Recent plate velocities from space geodesy, *J. geophys. Res.*, **107**, doi:10.1029/2000JB000033.
- Shapiro, N.M., Ritzwoller, M.H., Molnar, P. & Levin, V., 2004. Thinning and flow of Tibetan crust constrained by seismic anisotropy, *Science*, **305**, 233–236.
- Shen, F., Royden, L.H. & Burchfiel, B.C., 2001. Large-scale crustal deformation of the Tibetan Plateau, *J. geophys. Res.*, **106**, 6793–6816.
- Shen, Z.-K., Lu, J., Wang, M. & Burgmann, R., 2005. Contemporary crustal deformation around the southeast borderland of the Tibetan Plateau, *J. geophys. Res.*, **110**, doi:10.1029/2004JB003421.
- Shu, X.X., 1995. The genesis of Cpx-peridotite xenoliths in basanite of Maguan, Yunnan province, *Acta Petrol. Mineral.*, **14**, 47–51.

- Socquet, A., Vigny, C., Chamot-Rooke, N., Simons, W., Rangin, C. & Ambrosius, B., 2006. India and Sunda plates motion and deformation along their boundary in Myanmar determined by GPS, *J. geophys. Res.*, **111**, doi:10.1029/2005JB003877.
- Tilmann, F., Ni, J. & INDEPTH III Seismic Team, 2003. Seismic imaging of the downwelling Indian lithosphere beneath Central Tibet, *Science*, **300**, 1424–1427.
- Unsworth, M.J., Jones, A.G., Wei, W., Marquis, G., Gokarn, G., Spratt, J.E. & INDEPTH-MT team, 2005. Crustal rheology of the Himalaya and Southern Tibet inferred from magnetotelluric data, *Nature*, **438**, 78–81.
- Verma, R.K., Mukhopadhyay, M. & Ahluwalia, M.S., 1976. Seismicity, gravity, and tectonics of northeast India and northern Burma, *Bull. seism. Soc. Am.*, **66**, 1683–1694.
- Wang, J.-H., Yin, A., Harrison, T.M., Grove, M., Zhang, Y.-Q. & Xie, G.-H., 2001. A tectonic model for Cenozoic igneous activities in the eastern Indo-Asian collision zone, *Earth planet. Sci. Lett.*, **188**, 123–133.
- Wessel, P. & Smith, W.H.F., 1995. New version of the Generic Mapping Tools released, *EOS, Trans. Am. geophys. Un.*, **76**, 329.
- Zhang, P.-Z. *et al.*, 2004. Continuous deformation of the Tibetan Plateau from global positioning system data, *Geology*, **32**, 809–812.
- Zhao, W.-L. & Morgan, W.J., 1987. Injection of Indian crust into Tibetan lower crust: a two-dimensional finite element model study, *Tectonics*, **6**, 489–504.
- Zhou, H., Liu, H.L. & Kanamori, H., 1983. Source processes of large earthquakes along the Xianshuihe fault in southwestern China, *Bull. seism. Soc. Am.*, **73**, 537–551.

APPENDIX A: DETERMINATION OF EARTHQUAKE DEPTHS

In this appendix we describe the procedure used to determine the hypocentral depth of four earthquakes which occurred below the Indo–Burman Ranges. Due to the small magnitudes of the earthquakes (Table A1), and the resulting poor signal to noise ratio, we were unable to undertake a full inversion for source mechanism, depth and moment. We therefore only determined the depth, by performing forward modelling of vertical component of broadband seismograms using the program WKBJ3 (Chapman 1978). This program produces synthetic seismograms by tracing rays through a spherically symmetric earth from a given source depth and mechanism. We used the AK135 earth model (Kennett *et al.* 1995). We computed synthetics for the P , pP and sP phases using the focal mechanism from the CMT catalogue. These synthetics were convolved with the instrument responses of the receiving stations and corrected for attenuation using a Futterman operator with $t^* = 1$. The synthetic seismograms thus produced were then compared with actual seismograms, and the depth of the synthetic source varied to find the best match. The synthetic is scaled to the data using the rms amplitudes of the two traces, so it is the relative, rather than absolute, magnitudes of the signals which are considered when find-

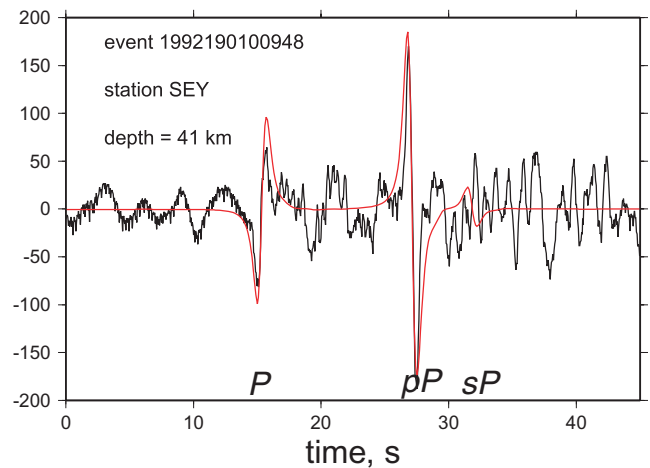


Figure A1. Real (black) and synthetic (red) vertical seismograms for the event 1992190100948 at station SEY. The synthetic is computed using a source depth of 41 km.

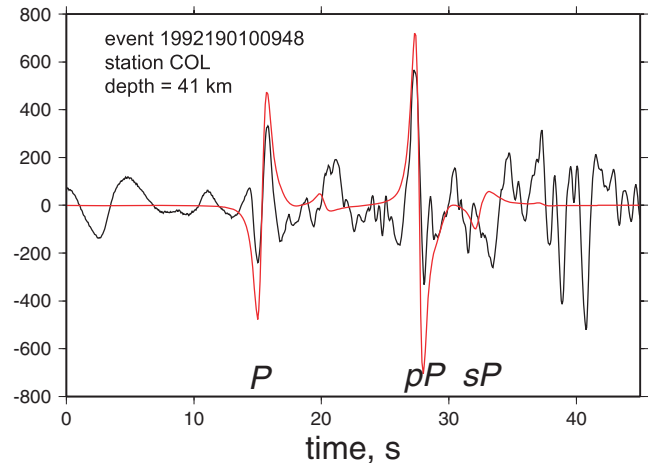


Figure A2. Real (black) and synthetic (red) vertical seismograms for the event 1992190100948 at station COL. The synthetic is computed using a source depth of 41 km.

ing the best fit. Figs A1–A11 show the data (black) overlain with the synthetic seismogram (red) for the earthquakes we have studied. The phases P , pP and sP have been labelled. For the 1997 event, for which we have determined a depth of 5 km, the arrivals of these phases overlap. Three stations have been shown for the earthquakes in 1992, 1997 and 2001 (Table A1), and two stations for the 1999 event.

Table A1. Details of the four earthquakes for which we have determined the depths. Position, source mechanism, and magnitude are taken from the CMT catalogue. EHB depth refers to the depth in the catalogue of Engdahl *et al.* (1998).

Year	Longitude	Latitude	Strike	Dip	Rake	M_w	CMT depth	EHB depth	Depth (this study)
1992	93.51	21.07	191	33	–75	5.2	79	57	41
1997	93.43	23.80	330	16	40	5.2	42	17	5
1999	93.99	23.15	47	35	–103	5.0	51	54	50
2001	93.43	23.99	140	40	–141	5.2	64	54	36

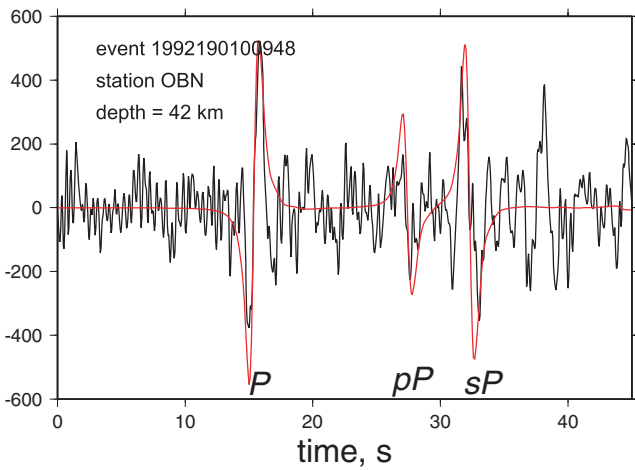


Figure A3. Real (black) and synthetic (red) vertical seismograms for the event 1992190100948 at station OBN. The synthetic is computed using a source depth of 42 km.

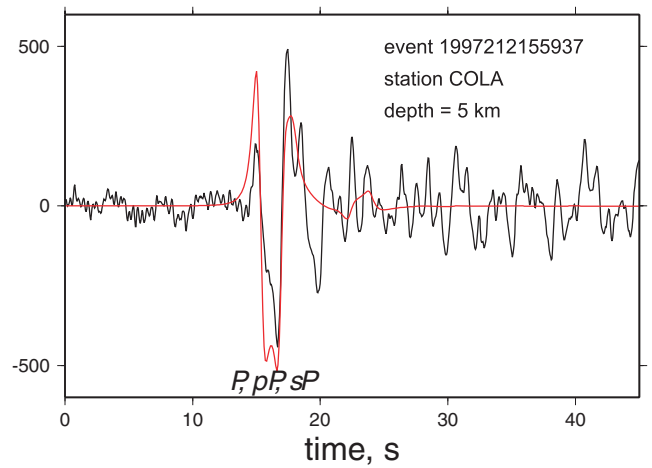


Figure A6. Real (black) and synthetic (red) vertical seismograms for the event 1997212155937 at station COLA. The synthetic is computed using a source depth of 5 km.

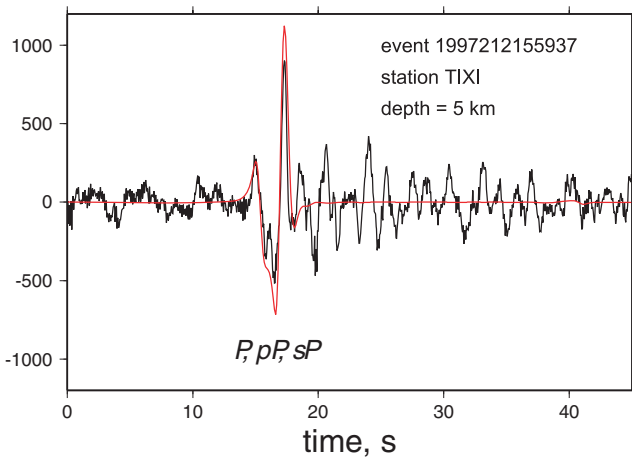


Figure A4. Real (black) and synthetic (red) vertical seismograms for the event 1997212155937 at station TIXI. The synthetic is computed using a source depth of 5 km.

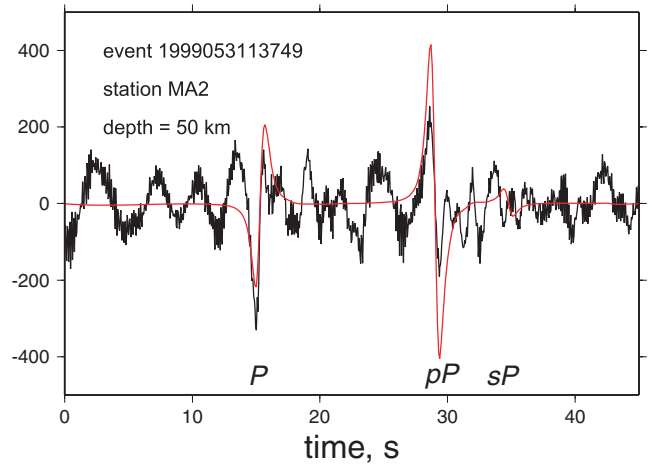


Figure A7. Real (black) and synthetic (red) vertical seismograms for the event 1999053113749 at station MA2. The synthetic is computed using a source depth of 50 km.

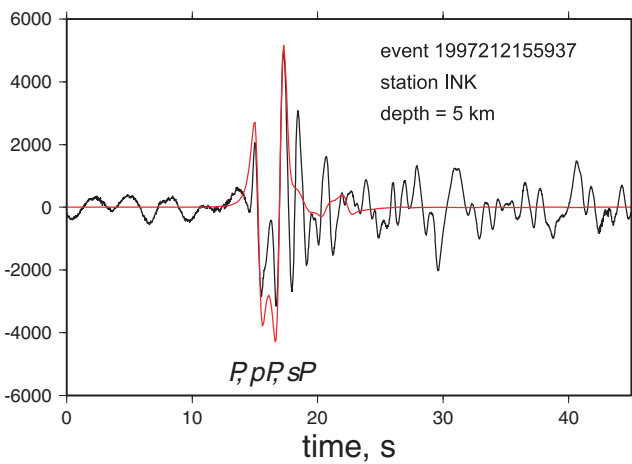


Figure A5. Real (black) and synthetic (red) vertical seismograms for the event 1997212155937 at station INK. The synthetic is computed using a source depth of 5 km.

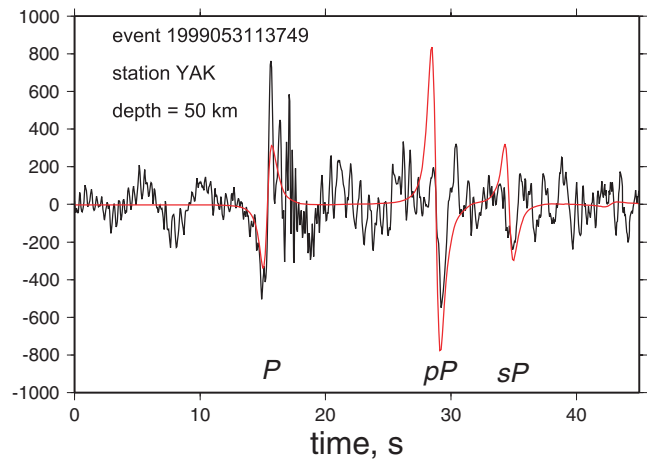


Figure A8. Real (black) and synthetic (red) vertical seismograms for the event 1999053113749 at station YAK. The synthetic is computed using a source depth of 50 km.

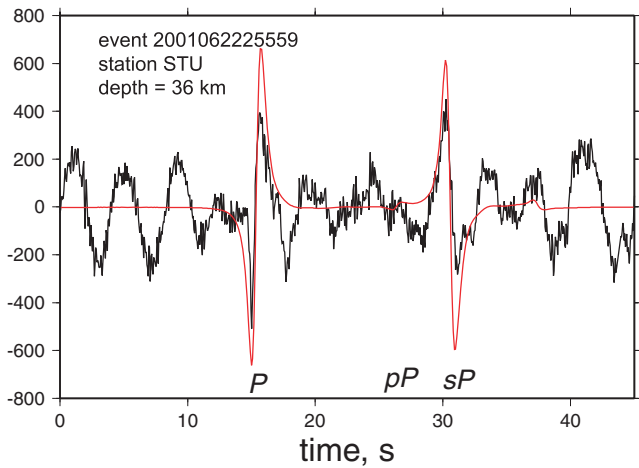


Figure A9. Real (black) and synthetic (red) vertical seismograms for the event 2001062225559 at station STU. The synthetic is computed using a source depth of 36 km.

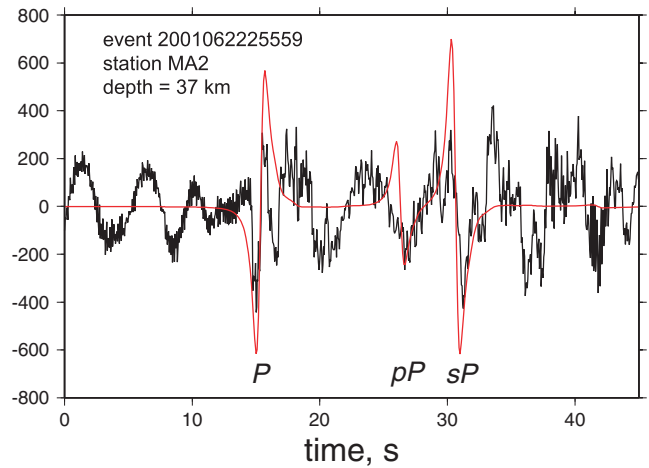


Figure A11. Real (black) and synthetic (red) vertical seismograms for the event 2001062225559 at station MA2. The synthetic is computed using a source depth of 37 km.

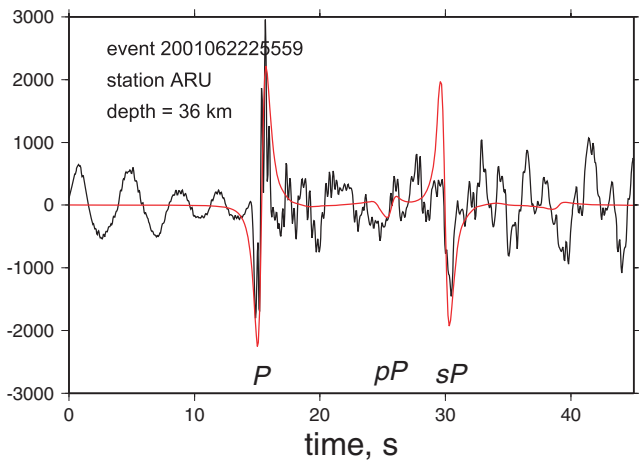


Figure A10. Real (black) and synthetic (red) vertical seismograms for the event 2001062225559 at station ARU. The synthetic is computed using a source depth of 36 km.

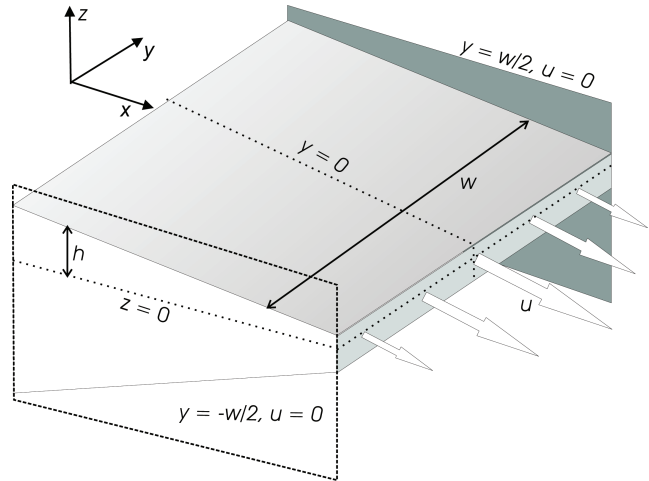


Figure B1. The coordinate system used in the derivation of eq. (3).

APPENDIX B: DERIVATION OF EQUATION 3

Fig. B1 shows the geometry of the flow. We consider a power-law fluid with a constitutive equation of the form

$$\tau_{ij} = BE^{\frac{1}{n}-1}\dot{\epsilon}_{ij}, \tag{B1}$$

where τ_{ij} are the components of the deviatoric stress tensor, $\dot{\epsilon}_{ij}$ are the components of the strain-rate tensor, E is the second invariant of the strain-rate tensor, given by $\sqrt{\dot{\epsilon}_{ij}\dot{\epsilon}_{ij}}$, and B and n are constant for a given material. We assume that the velocity in the x direction (u) varies only in the y direction (which implicitly assumes that the upper and lower boundaries are stress-free), and that the other velocity gradients are small compared to $\partial u/\partial y$. This allows us to simplify the expression for E and write

$$\tau_{xy} = \frac{B}{2\sqrt{2}^{1/n-1}} \left(\frac{\partial u}{\partial y}\right)^{\frac{1}{n}}. \tag{B2}$$

Momentum balance, neglecting inertial terms and assuming τ_{xy} is significantly larger than τ_{xx} and τ_{xz} (the latter of which is true because of the stress-free upper and lower boundaries), gives

$$\frac{\partial P}{\partial x} = \frac{\partial \tau_{xy}}{\partial y}. \tag{B3}$$

We assume that the velocity profile is symmetric about the x axis, which means that

$$\left(\frac{\partial u}{\partial y}\right)_{y=0} = 0. \tag{B4}$$

The second boundary condition is given by the zero-velocity conditions on the walls, so

$$(u)_{y=\pm w/2} = 0, \tag{B5}$$

where w is the width of the flow. Substituting (B2) into (B3) and solving for u using (B4) and (B5) gives

$$u = \left(\frac{\sqrt{2}^{1/n-1}}{B} \frac{\partial P}{\partial x}\right)^n \left(\frac{y^{n+1} - (w/2)^{n+1}}{n+1}\right). \tag{B6}$$